JCI The Journal of Clinical Investigation

Amendment history:
- Corrigendum (April 2013)

Impaired autophagic flux mediates acinar cell vacuole formation and trypsinogen activation in rodent models of acute pancreatitis

Olga A. Mareninova, … , Ilya Gukovsky, Anna S. Gukovskaya

J Clin Invest. 2009;119(11):3340-3355. https://doi.org/10.1172/JCI38674.

Research Article **Gastroenterology**

The pathogenic mechanisms underlying acute pancreatitis are not clear. Two key pathologic acinar cell responses of this disease are vacuole accumulation and trypsinogen activation. We show here that both result from defective autophagy, by comparing the autophagic responses in rodent models of acute pancreatitis to physiologic autophagy triggered by fasting. Pancreatitis-induced vacuoles in acinar cells were greater in number and much larger than those induced with fasting. Degradation of long-lived proteins, a measure of autophagic efficiency, was markedly inhibited in in vitro pancreatitis, while it was stimulated by acinar cell starvation. Further, processing of the lysosomal proteases cathepsin L (CatL) and CatB into their fully active, mature forms was reduced in pancreatitis, as were their activities in the lysosome-enriched subcellular fraction. These findings indicate that autophagy is retarded in pancreatitis due to deficient lysosomal degradation caused by impaired cathepsin processing. Trypsinogen activation occurred in pancreatitis but not with fasting and was prevented by inhibiting autophagy. A marker of trypsinogen activation partially localized to autophagic vacuoles, and pharmacologic inhibition of CatL increased the amount of active trypsin in acinar cells. The results suggest that retarded autophagy is associated with an imbalance […]

Impaired autophagic flux mediates acinar cell vacuole formation and trypsinogen activation in rodent models of acute pancreatitis

Olga A. Mareninova,[1] Kip Hermann,[1] Samuel W. French,[2] Mark S. O'Konski,[3] Stephen J. Pandol,[1] Paul Webster,[4] Ann H. Erickson,[5] Nobuhiko Katunuma,[6] Fred S. Gorelick,[7] Ilya Gukovsky,[1] and Anna S. Gukovskaya[1]

[1]Veterans Affairs Greater Los Angeles Healthcare System and University of California at Los Angeles, Los Angeles, California, USA. [2]Harbor-UCLA Medical Center, Torrance, California, USA. [3]Digestive Health Physicians, Fort Myers, Florida, USA. [4]House Ear Institute, Los Angeles, California, USA. [5]University of North Carolina, Chapel Hill, North Carolina, USA. [6]Tokushima Bunri University, Tokushima-city, Japan. [7]Veterans Affairs Medical Center and Yale University, West Haven, Connecticut, USA.

The pathogenic mechanisms underlying acute pancreatitis are not clear. Two key pathologic acinar cell responses of this disease are vacuole accumulation and trypsinogen activation. We show here that both result from defective autophagy, by comparing the autophagic responses in rodent models of acute pancreatitis to physiologic autophagy triggered by fasting. Pancreatitis-induced vacuoles in acinar cells were greater in number and much larger than those induced with fasting. Degradation of long-lived proteins, a measure of autophagic efficiency, was markedly inhibited in in vitro pancreatitis, while it was stimulated by acinar cell starvation. Further, processing of the lysosomal proteases cathepsin L (CatL) and CatB into their fully active, mature forms was reduced in pancreatitis, as were their activities in the lysosome-enriched subcellular fraction. These findings indicate that autophagy is retarded in pancreatitis due to deficient lysosomal degradation caused by impaired cathepsin processing. Trypsinogen activation occurred in pancreatitis but not with fasting and was prevented by inhibiting autophagy. A marker of trypsinogen activation partially localized to autophagic vacuoles, and pharmacologic inhibition of CatL increased the amount of active trypsin in acinar cells. The results suggest that retarded autophagy is associated with an imbalance between CatL, which degrades trypsinogen and trypsin, and CatB, which converts trypsinogen into trypsin, resulting in intra-acinar accumulation of active trypsin in pancreatitis. Thus, deficient lysosomal degradation may be a dominant mechanism for increased intra-acinar trypsin in pancreatitis.

Introduction

Autophagy (more precisely, *macroautophagy*) is a sequential process through which cells degrade long-lived proteins and cytoplasmic organelles, providing their constituents for recycling (1–3). Organelles destined for degradation are first sequestered in vacuoles called autophagosomes, which then fuse with late endosomes, forming amphisomes, and finally with lysosomes, forming autolysosomes. Material within autolysosomes is degraded by hydrolases, the most important class of which is the cathepsin family of proteases (4, 5). Cathepsins, such as cathepsin L (CatL) and CatB, undergo proteolytic processing during their transit from the Golgi complex to lysosomes, to become mature active enzymes (6–9). Autophagy is an adaptive response; starvation is one of its strongest physiological triggers. In response to starvation, autophagy mediates degradation of nonessential components and thus generates vital nutrients, such as amino acids (1, 3). Defects in the initiation of autophagy or its progression/resolution ("autophagic flux") are associated with a number of disorders, most prominently neurodegenerative diseases (3, 10, 11).

Pancreatitis is a potentially lethal inflammatory disease of the pancreas. Its pathogenesis remains obscure and specific treatments have not been developed. Accumulation of large vacuoles in acinar cells is a prominent and early feature of pancreatitis (12–18); however, the nature of these vacuoles, their mechanism of formation, and their relation to other pathological responses of pancreatitis have not been established. Another early response of pancreatitis is the pathological, intra-acinar cell activation of digestive enzymes, especially trypsinogen. Trypsinogen activation (i.e., its conversion from inactive zymogen to trypsin) has been found clinically and in experimental models of acute pancreatitis and is considered a critical disease-initiating event (19–24). The mechanism of the intra-acinar trypsinogen activation remains poorly understood. The current paradigm (19, 22, 23) is that it is catalyzed by CatB that has "missorted" and thus becomes colocalized with trypsinogen in as yet unidentified compartment(s).

The role of autophagy and its possible defects in pancreatitis is only starting to be elucidated. In particular, a recent study (25) using mice deficient in Atg5, a key autophagy protein, proposed that excessive autophagy is the cause of intra-acinar trypsinogen activation.

In the present study, we provide evidence that autophagy is impaired in pancreatitis and that impaired autophagy mediates both acinar cell vacuolation and the pathological, intra-acinar trypsin accumulation. We used in vivo and in vitro experimental models to show that autophagy is activated by both pancreatitis and fasting, but, unlike fasting, acute pancreatitis causes inhibition of lysosomal degradation and retardation of autophagic flux. We further found that pancreatitis impairs processing/maturation

Authorship note: Ilya Gukovsky and Anna S. Gukovskaya contributed equally to this work.

Conflict of interest: The authors have declared that no conflict of interest exists.

Citation for this article: *J. Clin. Invest.* **119**:3340–3355 (2009). doi:10.1172/JCI38674.

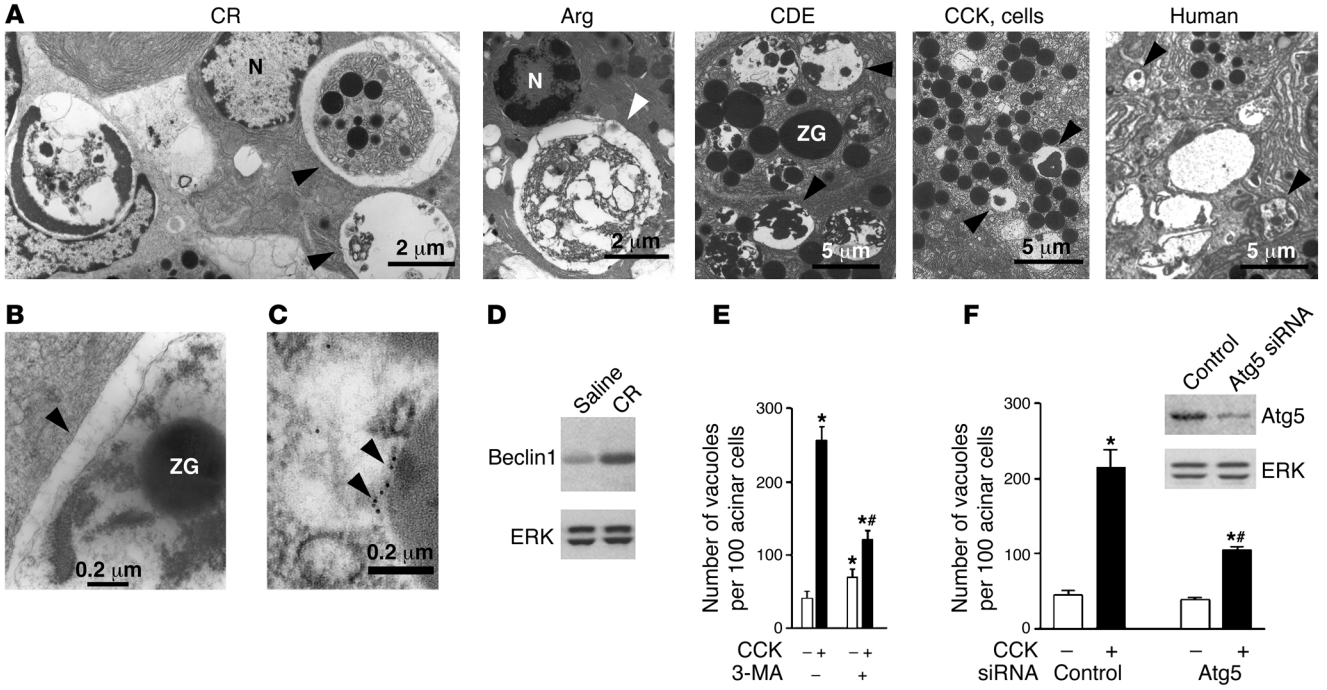

Figure 1
Autophagy is activated in acute pancreatitis and is involved in acinar cell vacuolation. (**A**) Electron micrographs showing autophagic vacuoles (arrowheads) in pancreatic tissue (or isolated acinar cells) from experimental models of pancreatitis (see Methods) and in pancreas of a patient with acute pancreatitis. Shown is pancreatitis induced in rats by CR or Arg, in mice by CDE, and the in vitro model of acinar cells hyperstimulated with CCK. N, nucleus. Larger fields and higher-magnification images are shown in Supplemental Figure 1. (**B**) Electron micrograph demonstrating the double membrane (arrowhead), a characteristic of autophagosomes, in CR pancreatitis. (**C**) Electron micrograph illustrating LC3 immunogold localization (arrowheads) to an autophagic vacuole in pancreas of a GFP-LC3 transgenic mouse with CR pancreatitis. (**D**) Pancreatic level of beclin1 increased in CR pancreatitis (immunoblot). ERK1/2 served as loading control. (**E** and **F**) Inhibiting autophagy with 3-MA or Atg5 siRNA greatly decreased vacuolation in acinar cells hyperstimulated with CCK. (**E**) Rat acinar cells were incubated for 3 hours with or without 100 nM CCK and 10 mM 3-MA. Vacuoles were counted in cells stained with toluidine blue. (**F**) Mouse acinar cells were transfected with Atg5 siRNA or control siRNA (see Methods), and then incubated for 3 hours with and without 100 nM CCK. The inset illustrates transfection efficiency. Cells were immunostained for LC3, and vacuoles (LC3 dots) were counted under confocal microscope using ImageJ software. Values (mean ± SEM) are from at least 1,000 cells for each condition (**E** and **F**). $^{*}P < 0.05$ versus control cells; $^{\#}P < 0.05$ versus CCK alone.

and activities of CatL and CatB, which may underlie the inefficient lysosomal degradation. Our results indicate that this dysfunction, rather than missorting of Cat B (19, 22, 23) or excessive autophagy (25), mediates the intra-acinar accumulation of active trypsin.

Results

Autophagic flux is impaired in acute pancreatitis

Autophagy is activated and is involved in vacuole accumulation in acinar cells, a key pathological response of acute pancreatitis. We first examined acinar cell vacuolation in different experimental models of pancreatitis as well as in human tissue with EM (Figure 1, A–C; see larger fields in the Supplemental Figure 1; supplemental material available online with this article; doi:10.1172/JCI38674DS1). Numerous vacuoles containing nondegraded or partially degraded material (including zymogen granules [ZGs]) were seen in acinar cells in all models examined (see Methods), namely pancreatitis induced in rats by cerulein (CR) or L-arginine (Arg); in mice, by feeding them choline-deficient, ethionine-supplemented diet (CDE); and in isolated acinar cells hyperstimulated with CCK-8 (CCK) (in vitro model of pancreatitis). Vacuoles with partially degraded cellular material were also seen on electron micrographs of human pancreas from a patient with acute pancreatitis (Figure 1A and Supplemental Figure 1). Of note, these vacuoles were often large, even larger than the nucleus (e.g., in CR and Arg pancreatitis). The presence of partially digested material is a hallmark of autophagic vacuoles (1, 3, 26). Also, the vacuoles accumulated in pancreatitis have double membranes (Figure 1B), another characteristic of autophagic vacuoles (2, 26, 27). Further, immunogold EM (Figure 1C) demonstrated the presence of the microtubule-associated protein 1 light chain 3 (LC3; the mammalian ortholog of yeast Atg8), a specific marker of autophagic vacuoles (28), in pancreatic acinar cells. Of note, acinar cells in pancreatitis contained both of the 2 morphologically distinct types of vacuoles that are classified in autophagy research as early, initial autophagic vacuoles (AVi; mostly autophagosomes), containing intact sequestered material, and late, degradative autophagic vacuoles (AVd; mostly autolysosomes), containing partially degraded but identifiable cargo (1, 29). As shown in Figure 1A, the CR pancreatitis panel presents examples of both types of autophagic vacuoles in the same acinar cell.

As further evidence that autophagy is activated in pancreatitis, we showed by immunoblot that pancreatic level of beclin1 (Atg6), a key autophagy mediator (1, 2), greatly increased in CR pancreatitis (Figure 1D).

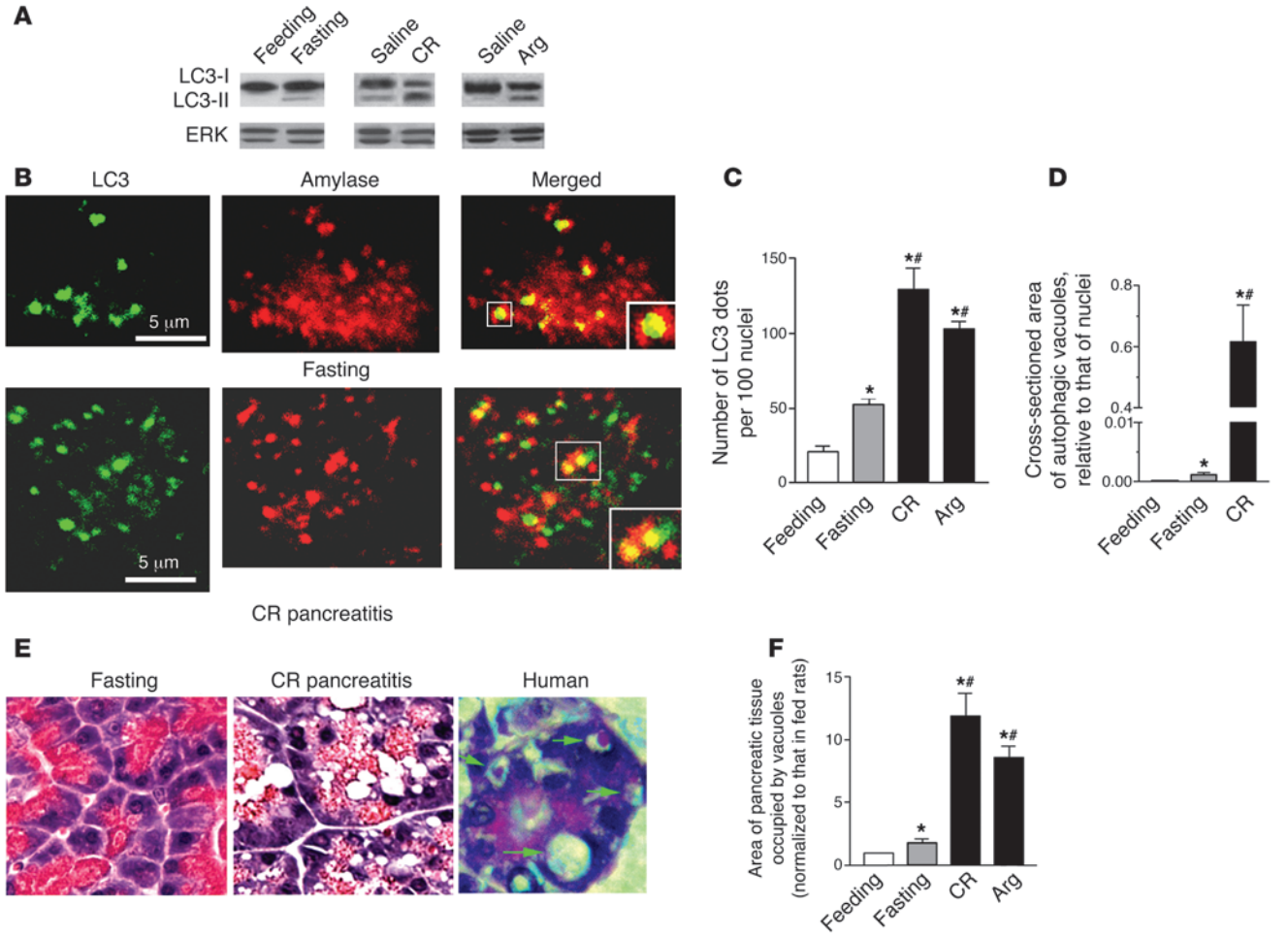

Figure 2

Compared with fasting, pancreatitis-induced autophagic vacuoles are greater in number and much larger. (**A**) LC3-I to LC3-II conversion (immunoblot) in pancreas of rats under conditions of fasting (for 17 hours) and pancreatitis (see Methods). ERK1/2 served as loading control. (**B**) Colocalization of the autophagy marker LC3 with amylase, a ZG marker, under conditions of fasting and CR pancreatitis. Pancreatic tissue sections were double immunostained for LC3 and amylase. Images were visualized under confocal microscope. Larger boxes show expanded images of the areas indicated by smaller boxes. (**C**) Effects of fasting and pancreatitis on LC3 dots in pancreas, as shown in **B**. The number of LC3 dots was normalized to that of nuclei in the same field. (**D**) Autophagic vacuoles were identified on electron micrographs (see Figure 1), and their size was measured relative to the average size of nuclei on the same micrograph. (**E**) Acinar cell vacuolation on H&E-stained pancreatic tissue sections from rats under conditions of fasting or CR pancreatitis (original magnification, ×40) and from a patient with acute pancreatitis (a gift from D.S. Longnecker; original magnification, ×60). (**F**). Cross-sectioned area of pancreas occupied by vacuoles was quantified on H&E-stained sections using MetaMorph 6 software. Values in **C**, **D**, and **F** are (mean ± SEM) from 3–5 rats for each condition. In **C** and **F**, at least 1,000 acinar cells were counted for each animal. In **D**, 20–30 acinar cells from at least 3 rats were counted for each condition. $^{*}P < 0.05$ versus fed rats; $^{\#}P < 0.02$ versus fasting rats.

To quantify the contribution of autophagy to acinar cell vacuolation, we measured the effects on vacuole accumulation of blocking autophagy with a specific inhibitor, 3-methyladenine (3-MA), or by using siRNA against Atg5, a protein important for autophagy induction (2, 28). Both 3-MA (Figure 1E) and Atg5 siRNA transfection (Figure 1F) substantially inhibited acinar cell vacuolation induced by supramaximal CCK (the in vitro model of pancreatitis). These results are in accord with a recent study (25), showing that acinar cell vacuolation in CR pancreatitis was greatly inhibited in *Atg5*-deficient mice.

The results in Figure 1 (and those of ref. 25) indicate that autophagy is activated in acute pancreatitis and is involved in acinar cell vacuolation, a key pathological response of pancreatitis. Vacuole accumulation could be a result of enhanced autophagy or impaired progression/resolution (flux) of autophagy (3). Therefore, we asked whether acinar cell vacuolation — as well as other pathological responses — are caused by activation of autophagy or by its disordering in pancreatitis. For this purpose, we compared autophagy in models of pancreatitis with the "classic" physiological autophagy response induced by starvation (fasting). Of note, fasting has been recently shown (28) to potently activate autophagy in exocrine pancreas.

Compared with fasting, autophagic vacuoles induced by pancreatitis are greater in number and much larger. Western blot analysis showed that both fasting and pancreatitis stimulated LC3 conversion in pancreas from the cytosolic (~18 kDa) LC3-I to vesicular (~16 kDa)

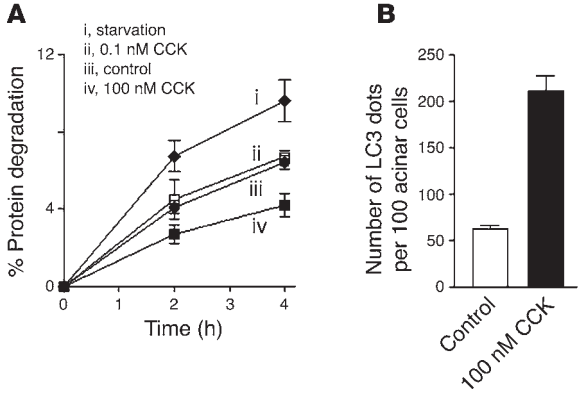

Figure 3

Starvation increases, but CCK hyperstimulation decreases autophagy-mediated protein degradation in pancreatic acinar cells. (**A**) Autophagy-mediated degradation of long-lived proteins was measured in mouse pancreatic acinar cells by pulse-chase assay, as described in Methods. Briefly, the culture medium was supplemented for the first 6 hours with [^{14}C]-valine to label proteins, after which cells were chased for 16 hours in fresh medium containing cold valine. Cells were then switched to either (ii–iv) medium 199 containing amino acids or (i) nutrient-free (i.e., free of amino acids) medium, and further cultured for 4 hours with 0.1 nM (ii) or 100 nM (iv) CCK, or without CCK (i and iii), both in the presence and absence of 10 mM 3-MA. Protein degradation was measured as the net release of TCA-soluble radioactivity; values obtained in the presence of 3-MA were subtracted as nonautophagic background. The measurements were in duplicates, and the experiment was repeated with similar results. Data represent mean ± SEM. (**B**) Quantification of LC3 dots in acinar cells incubated in conditions iii and iv described in **A** (that is, control versus 100 nM CCK). LC3 dots were visualized under confocal microscope as illustrated in Figure 2B and counted, with the use of ImageJ software, in at least 1,000 acinar cells for each condition. Values are mean ± SEM (n = 4).

LC3-II form, which uniquely marks the autophagosomal and amphisomal membranes (Figure 2A and Supplemental Figure 2). Similar results for mouse CR pancreatitis were reported in ref. 25. The extent of LC3 conversion in both CR and Arg pancreatitis was much greater than in pancreas of rats fasted overnight (Figure 2A) or up to 64 hours (Supplemental Figure 2). Of note, pancreatic LC3-II levels decreased rather than increased over the duration of fasting (Supplemental Figure 2).

As is commonly done, CR pancreatitis was induced in rats fasted overnight (for 17 hours). This approach, namely the use of overnight fasted animals, is applied in models of CCK- or CR-induced pancreatitis to avoid the effect of variable secretion during the nocturnal feeding period (e.g., refs. 30, 31). The extent of LC3 conversion in pancreas (as well as other parameters of autophagy) was similar in rats either fasted for 17–24 hours or fasted overnight and then used as saline-injected controls for CR pancreatitis (Figure 2A).

Both fasting and pancreatitis increased the number of punctate, vesicular LC3-immunopositive structures ("LC3 dots"; ref. 27) in pancreas. LC3 dots in pancreas partly colocalized with amylase, a major digestive enzyme contained in ZGs of acinar cells (Figure 2B). This confirms EM data (Figure 1A and Supplemental Figure 1), demonstrating ZGs sequestered within autophagic vacuoles. In both CR and Arg pancreatitis, the number of LC3 dots representing autophagic vacuoles increased 2.0–2.5 times more than that with fasting (Figure 2C). Using transgenic GFP-LC3 mice (28), we confirmed that the increase in the number of GFP-LC3 dots was much greater in CR pancreatitis than that with fasting (data not shown).

Autophagic vacuoles induced by pancreatitis and fasting exhibited a striking difference in size. EM showed that the average cross-sectional area of autophagic vacuoles in pancreas of rats with CR pancreatitis was more than 100 times larger than those in fasting conditions (Figure 2D). In agreement with the EM data, quantification of total vacuoles on H&E-stained pancreatic tissue sections showed that both their number and the area occupied by vacuoles were much greater in CR or Arg pancreatitis than with fasting (Figure 2, E and F; and data not shown).

Autophagy-mediated degradation of long-lived proteins is inhibited in the in vitro model of pancreatitis. Accumulation of large autophagic vacuoles could be an indication of impaired flux through autophagy pathway, that is, impaired progression from autophagosomes to autolysosomes and inefficient autophagic protein clearance (3). To address this issue, we measured the rate of long-lived protein degradation, a key parameter of autophagy efficiency (27), in conditions of in vitro pancreatitis (Figure 3). For this assay (see Methods), we used prolonged primary culture of mouse pancreatic acinar cells (32), described in detail in Methods. Cells were first cultured for 6 hours in the presence of [^{14}C]-valine to label proteins and then chased for 16 hours in fresh medium containing "cold" valine. Cells were then incubated with either physiological (10 pM) or supramaximally stimulating (100 nM) CCK (as well as vehicle) in both the regular 199 medium (containing amino acids) or a nutrient-free medium (devoid of amino acids), which is commonly used for "in vitro starvation" experiments (33). This experimental design aimed to measure the effects of physiological versus supramaximal CCK and compare those with that of amino acid withdrawal, which has been shown (33) to trigger autophagy responses and stimulate protein degradation in other cells. To determine the fraction of protein degradation that is autophagy independent, parallel incubations were performed for each condition in the presence or absence of the autophagy inhibitor 3-MA (10 mM) (27). Subtracting the values obtained in the presence of 3-MA (from those obtained without 3-MA) provides the autophagy-mediated net rate of long-lived protein degradation.

These experiments yielded several salient findings (Figure 3, A and B). First, starvation (i.e., nutrient-free medium) increased the rate of autophagy-mediated protein degradation in acinar cells approximately 1.7 fold. This increase, as well as the basal rate of protein degradation (~7% over 4 hours), is similar to that reported for other cell types (34). Second, whereas the physiological CCK concentration slightly stimulated protein degradation, the supramaximal CCK markedly inhibited autophagy-mediated protein degradation in acinar cells (Figure 3A). Third, the autophagy-independent ("3-MA resistant") part of protein degradation was the same in all 4 conditions, at both 2-hour and 4-hour time points; that is, it was not affected by CCK. Finally, the CCK-induced inhibition of protein degradation was associated with accumulation of LC3-positive vacuoles in acinar cells (Figure 3B). Thus, CCK hyperstimulation of acinar cells (in vitro model of pancreatitis) caused a decrease in protein degradation, concomitant with accumulation of autophagic vacuoles. These findings strongly indicate that in contrast to starvation, efficient progression of autophagy (autophagic flux) is impaired in pancreatitis.

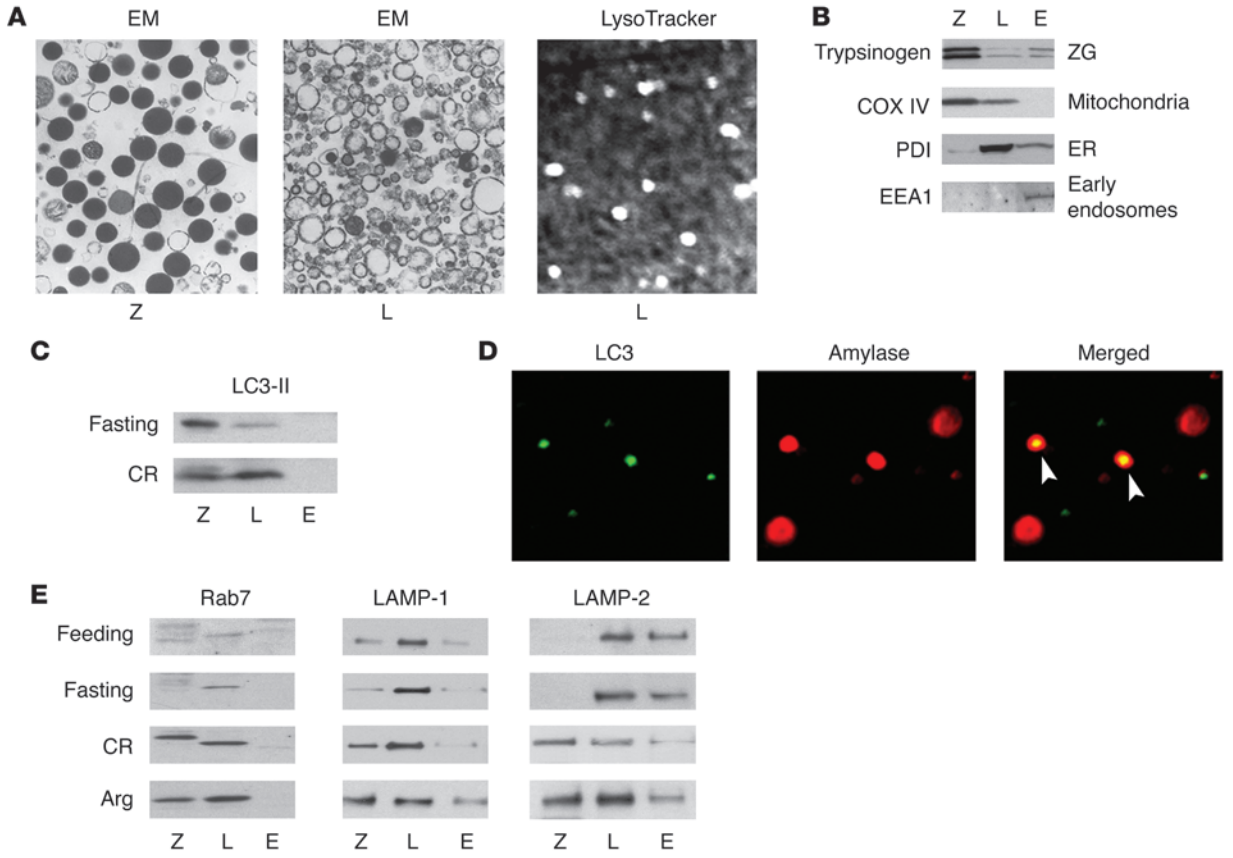

Figure 4

In pancreatitis, lysosomal markers accumulate in a heavier, ZG-enriched subcellular fraction. (**A** and **B**) Characterization of pancreatic tissue subcellular fractions. Rat pancreas homogenate was fractionated by differential centrifugation, as described in Methods, to obtain 1,300-*g* pellet enriched in ZGs (fraction Z [Z]); 12,000-*g* pellet enriched in lysosomes (fraction L [L]); and 12,000-*g* supernatant containing early endosomes and cytosolic proteins (fraction E [E]). (**A**) The indicated subcellular fractions were analyzed under electron microscope or under fluorescence microscope using the lysosomal vital stain LysoTracker Red. Original magnification: ×7,500 (left panel); ×12,500 (center panel); ×40 (right panel). Larger EM fields are shown in the Supplemental Figure 3. (**B**) Subcellular fractions from normal rat pancreas were analyzed by immunoblot using antibodies against proteins specific for the organelles listed to the right. COX IV, cytochrome c oxidase subunit IV; PDI, protein disulfide isomerase; EEA1, early endosomal antigen. (**C** and **E**) Rats were subjected to conditions of fasting and pancreatitis induced by CR or Arg, as described in Methods. The levels of LC3-II, Rab7, LAMP-1, and LAMP-2 were measured by immunoblot in pancreatic tissue subcellular fractions. For each protein, the same amount of protein was loaded in all samples. The data are representative of several immunoblots from at least 3 rats for each condition. (**D**) Colocalization of the autophagic marker LC3 with amylase in fraction Z, obtained from a rat with CR pancreatitis, was determined by double staining with anti-LC3 antibody and FITC-conjugated secondary antibody (for LC3 dots) and with amylase antibody and Texas Red–conjugated secondary antibody. Original magnification: ×63.

In pancreatitis, lysosomal markers accumulate in the heavier, ZG-enriched subcellular fraction. To further examine the effects of pancreatitis on autophagic flux, we studied the distribution of lysosomal markers in subcellular fractions obtained from pancreas of rats subjected to pancreatitis or fasting (Figure 4 and Supplemental Figure 3). The method of pancreatic tissue fractionation was introduced more than 30 years ago (35) and modified by Steer and Saluja (30, 36). Briefly, pancreatic tissue homogenate was subjected to differential centrifugation to form 3 fractions: (a) 1,300-*g* pellet, which was enriched in ZGs (fraction Z); (b) 12,000-*g* pellet, which was enriched in lysosomes (fraction L); and (c) 12,000-*g* supernatant, containing early endosomes, ER, and cytosolic proteins (fraction E). In accordance with the published EM data (36), we confirmed (Figure 4A; see larger fields in Supplemental Figure 3) that in our preparations from normal rat pancreas, fraction Z was greatly enriched in ZGs and also contained mitochondria, while fraction L contained lysosomes, some mitochondria, and mostly ER. We further visualized lysosomes in fraction L, by using the specific vital stain LysoTracker Red (Figure 4A). The LysoTracker staining, as well as staining of mitochondria with another vital probe, MitoTracker Red (data not shown), confirmed that our preparations contained intact organelles.

To further characterize the nature of the subcellular fractions, we used Western blot analysis to detect markers specific for different organelles. The results (Figure 4B) are consistent with the EM data (Supplemental Figure 3) and demonstrate, for example, that trypsinogen, a major zymogen, was enriched in fraction Z and also present in fraction E; fraction Z contained little ER; and early endosomes were only present in fraction E. The vesicular material in fraction E is also shown by EM (Supplemental Figure 3). LC3-II immunoblot showed that autophagic vacuoles are in fractions Z and L (Figure 4C). Colocalization of punctate LC3 with amylase

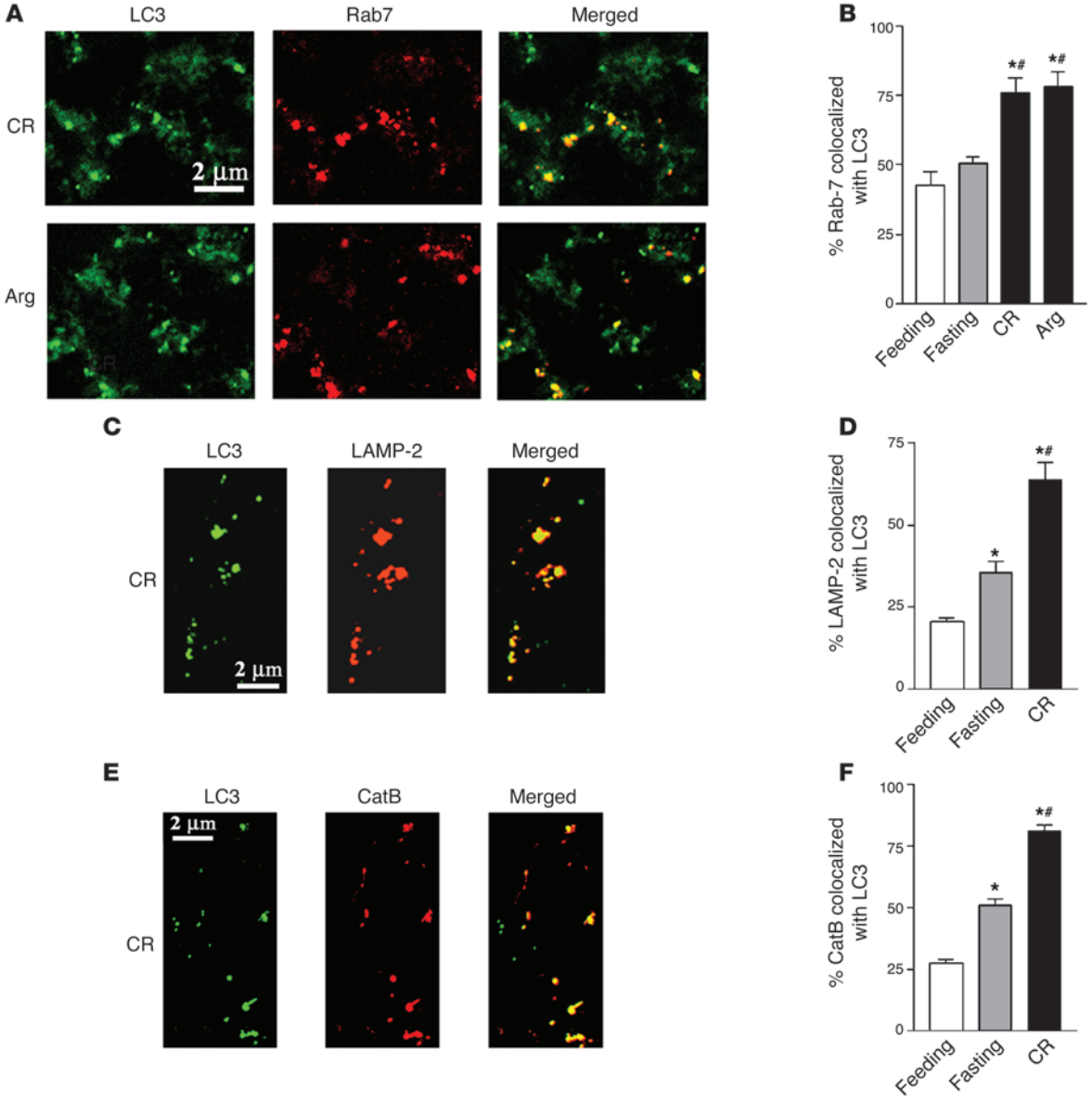

Figure 5

Colocalization of lysosomal markers Rab7, LAMP-2, or CatB with the autophagosomal marker LC3 increases in models of pancreatitis. Rats were subjected to conditions of fasting and pancreatitis induced by CR or Arg, as described in Methods. (**A**, **C**, and **E**). Pancreatic tissue sections were double stained with anti-LC3 antibody and FITC-conjugated secondary antibody (for LC3 dots) and with a primary antibody against Rab7 (**A**), LAMP-2 (**C**), or CatB (**E**) and Texas Red-conjugated secondary antibody. Images were visualized under confocal microscope. (**B**, **D**, and **F**). Colocalization of Rab7, LAMP-2, or CatB with LC3 was quantified with the use of ImageJ software. Values are (mean ± SEM) from at least 3 animals for each condition. $^{*}P < 0.05$ versus normally fed rats; $^{\#}P < 0.05$ versus fasting rats.

in fraction Z, both in normal rat pancreas (data not shown) and CR pancreatitis (Figure 4D), further indicated that some of the autophagic vacuoles in fraction Z contain ZG.

We next measured the effects of fasting and pancreatitis on the subcellular distribution of the lysosome-associated membrane protein-1 (LAMP-1) and LAMP-2 as well as Rab7 (Figure 4E). LAMP-1 and LAMP-2 are major lysosomal integral membrane proteins but are also present in prelysosomal structures, whereas Rab7 is specific for lysosomes and late endosomes (29, 37). We found that fasting did not cause significant changes in the subcellular distribution of these proteins in pancreas, compared with that in fed rats. Thus, in both fed and fasted animals, the LAMPs and Rab7 were mostly in the lysosome-enriched fraction L (there was also a substantial amount of LAMP-2 in fraction E). In contrast, CR and Arg pancreatitis induced dramatic increases in all 3 proteins in the heavier, ZG-enriched fraction Z (Figure 4E). Notably, the apparent molecular weight of Rab7 localized to fraction Z in CR pancreatitis was different from that of the "basal" form of Rab7 protein present in fraction L (Figure 4E).

A logical explanation for the pancreatitis-induced shift of lysosomal markers to the heavier fraction Z is that it is caused by retarded autophagy progression, resulting in accumulation of

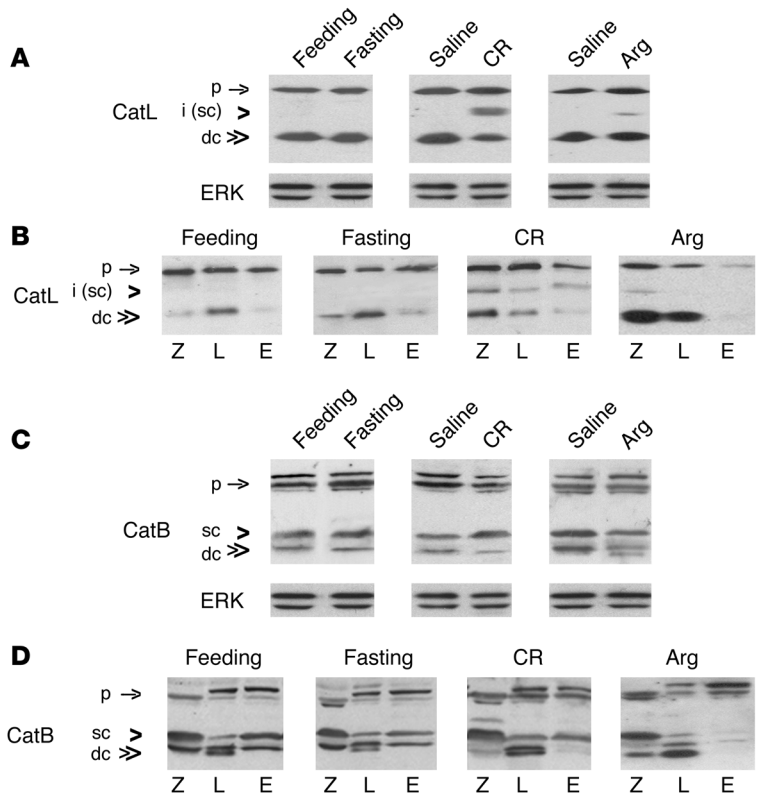

Figure 6
Pancreatitis but not fasting impairs processing/maturation of CatL and CatB. Rats were subjected to conditions of fasting and pancreatitis induced by CR or Arg, as described in Methods. Levels of CatL and CatB were measured by immunoblot in (**A** and **C**) whole pancreatic tissue or (**B** and **D**) pancreatic subcellular fractions, obtained as in Figure 4. ERK1/2 served as loading control. For each cathepsin, the same amount of protein was loaded in all samples. The data are representative of several immunoblots from at least 3 rats for each condition. p, cathepsin proform; i, intermediate form; sc, the single-chain form; dc, the fully processed, double-chain form.

heavy autolysosomes containing partially degraded cargo. This conclusion is consistent with our finding that pancreatitis causes inhibition of autophagic protein degradation and accumulation of large vacuoles in acinar cells (Figure 3). The dramatic increase in LC3-II level in fraction L observed in CR pancreatitis (Figure 4C) is also consistent with retarded autophagic flux.

Rab7 levels in whole pancreatic tissue were upregulated in both CR and Arg pancreatitis (Supplemental Figure 4), in accordance with the changes observed on subcellular fractions. Moreover, CR but not Arg pancreatitis caused a dramatic increase in both lower and upper bands of Rab7 doublet (Supplemental Figure 4), corresponding to the appearance of the higher-molecular-weight Rab7 band in fraction Z (Figure 4E). The effects of pancreatitis on total levels of LAMP-1 were less dramatic (Supplemental Figure 4) and in accordance with the results on subcellular fractions.

Pancreatitis does not block the fusion of autophagosomes with late endosomes/lysosomes. One possible explanation for the impaired autophagy progression in pancreatitis could be blockade of the fusion between autophagosomes and late endosomes/lysosomes, a common defect in lysosomal diseases (3, 10). However, this mechanism does not appear to account for the defect in pancreatitis. We found that the colocalization of the autophagosomal marker LC3-II with the lysosomal markers Rab7 or LAMP-2 (as well as with CatB) markedly increased in pancreatitis (Figure 5). Compared with that in feeding conditions, fasting did not change Rab7 colocalization with LC3 (Figure 5B), and it increased the colocalization of LAMP-2 (Figure 5D) and CatB (Figure 5F) with LC3 significantly less than pancreatitis.

The results in Figure 5 indicate that the fusion between autophagosomes and late endosomes/lysosomes was not blocked in pancreatitis. This is in agreement with our EM data that demonstrate a great number of vacuoles with partially degraded material in various models of pancreatitis (Figure 1 and Supplemental Figure 1). Thus, the data suggest that the defective autophagic protein degradation we observe in pancreatitis is not caused by a blockade of formation of autolysosomes but could be caused by decreased lysosomal function, that is, decreased activity of lysosomal hydrolases. To examine this issue, we assessed the effects of pancreatitis and fasting on the processing and activities of CatL and CatB, which are important for autophagic function (3). CatB is relevant for the mechanism of pancreatitis, because there is compelling evidence (19, 21, 22, 24, 38, 39) that it is a key activator of the pathological, intra-acinar conversion of trypsinogen to trypsin. Although CatL is present in human and rodent pancreas, there is little known on its role in pancreatitis (40–42).

Processing and activities of CatL and CatB are dysregulated in acute pancreatitis

Processing of CatL and CatB is impaired in pancreatitis, and active forms of CatL (but not CatB) accumulate in ZG-enriched subcellular fraction. Cathepsins are activated through sequential proteolytic cleavage of their inactive proform. First, they are partially processed into a "single-chain" form, which is then cleaved into a heavy and light chain. These, in turn, form a noncovalent complex ("double-chain" form), representing the fully mature cathepsin (5–8). Fully mature, double-chain cathepsins are usually formed in lysosomes, whereas partially processed (e.g., single-chain) active forms can also be present in prelysosomal structures (5, 9). Defects in cathepsin processing/maturation may lead to impaired lysosomal protein clearance, as observed in some neurodegenerative lysosomal disorders (10).

We examined the effects of pancreatitis and fasting on cathepsin processing by immunoblot (Figure 6), using antibodies that recognize the proform, the partially processed (single-chain) form, and the heavy chain of the fully matured (double-chain) CatL and CatB. (Of note, there are few examples of immunoblots for these cathepsins in tissues and almost none in pancreas [ref. 43].) Fasting did not cause significant changes in the band profile of CatL, either in the whole pancreatic tissue (Figure 6A) or subcellular fractions (Figure 6B). In pancreas of both fasted and fed rats, the active CatL was only present in its fully mature, double-chain (~25 kDa) form, which was predominantly in the lysosome-enriched fraction L.

In contrast, CR and Arg pancreatitis caused the appearance in rat pancreas of a partially processed form of CatL (Figure 6A). Based on its apparent molecular weight (~32 kDa), this intermedi-

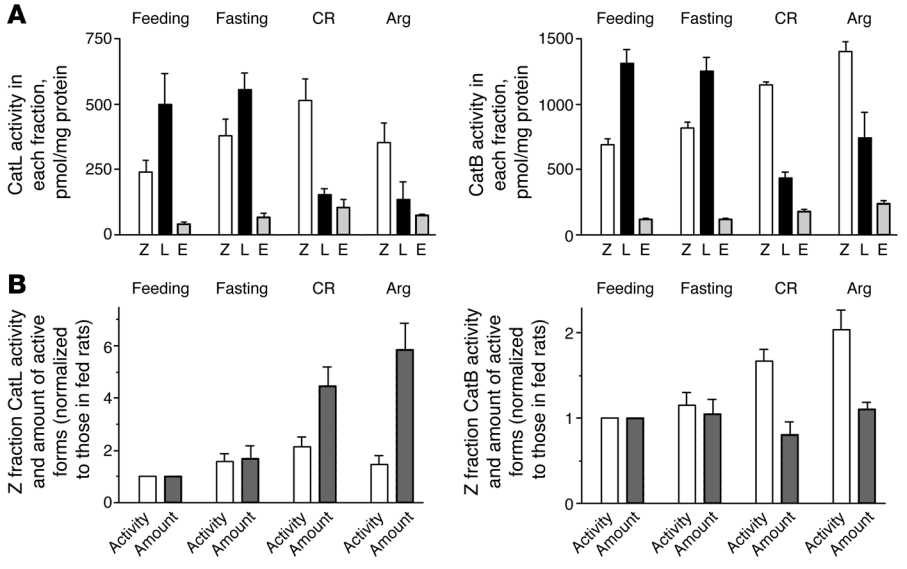

Figure 7
Effects of pancreatitis and fasting on CatL and CatB activities in subcellular fractions. Rats were subjected to conditions of fasting and pancreatitis induced by CR or Arg, as described in Methods, and pancreatic subcellular fractions were obtained as in Figure 4. (**A**) CatL and CatB activities were measured by a fluorogenic enzymatic assay and expressed per milligram of protein in each fraction. (**B**) Comparison of the changes in the activities of cathepsins in the ZG-enriched fraction Z versus the amount of their active (processed) forms in this fraction. The values of CatL and CatB activities shown in **A** were normalized to those for the feeding conditions. Changes in the amount of active (processed) forms of cathepsins in fraction Z were assessed from densitometric quantification of their immunoblots, as described in Methods. Values are (mean ± SEM) from at least 3 animals for each condition.

ate form likely represents the single-chain CatL. In CR pancreatitis, the intermediate form appeared in all 3 subcellular fractions, whereas in the Arg model, it was mostly in fraction Z (Figure 6B). Further, pancreatitis caused dramatic accumulation of active CatL forms, both the partially (single-chain form) and fully processed (double-chain form), in the ZG-enriched fraction Z (Figure 6B). In Arg pancreatitis, the increase in the double-chain CatL was not only in fraction Z but also L (Figure 6B). Another distinct effect of Arg pancreatitis was a CatL decrease in fraction E.

CatB band profiles in normal rat pancreas (Figure 6, C and D) were very different from CatL. First, CatB proform appeared on immunoblot as doublet or triplet bands; these multiple bands may correspond to forms varying in phosphorylation (44). Second, active (processed) CatB was present as both the single- and double-chain forms (based on their apparent molecular weight of ~31 and ~27 kDa, respectively). Third, the active forms of CatB were equally distributed in all 3 fractions (Figure 6D). Of note, the profile of CatB bands was distinct for each fraction. For example, in the lysosome-enriched fraction L there was more double- than single-chain CatB, and the double-chain form was manifest as a doublet (Figure 6D). (The doublet may represent heavy chains differing in the extent of glycosylation [ref. 45]. The distinct CatB band patterns in subcellular fractions indicate that there was little cross-contamination among the fractions.)

Fasting did not affect CatB processing, as shown by CatB band profiles in whole pancreas (Figure 6C) and subcellular fractions (Figure 6D). In contrast, in both models of pancreatitis, there was a decrease in the double-chain form of CatB in pancreas (Figure 6C). Arg pancreatitis displayed a decrease in both the double- and single-chain CatB forms. The subcellular fractions immunoblots (Figure 6D) showed that pancreatitis-induced decrease in the double-chain CatB was in fractions Z and E. In the Arg model, fraction E displayed a dramatic decrease in both the double- and single-chain CatB forms.

Thus, pancreatitis appears to affect the processing (maturation) of key lysosomal enzymes. The major effects on CatL were the appearance of its partially processed (single-chain) form and the accumulation of active CatL forms in the heavier, ZG-enriched fraction Z. The main effect of pancreatitis on CatB was a decrease in its fully mature form. Importantly, however, there was no redistribution of CatB from fraction L to Z in any model of pancreatitis. As shown in Figure 6, cathepsins processing/maturation is profoundly impaired in acute experimental pancreatitis, resulting in a shift toward immature CatL and CatB forms. Such impairment may cause deficient lysosomal protein clearance and retarded autophagic flux.

Pancreatitis but not fasting greatly decreases CatB and CatL activities in the lysosome-enriched subcellular fraction. Neither pancreatitis nor fasting markedly affected CatL and CatB activities in the whole pancreas, compared with those in fed conditions (data not shown). Previously, a similar result has been reported for CatB in CR pancreatitis (36). However, pancreatitis and fasting had dramatically different effects on activities of cathepsins in the subcellular fractions (Figure 7). Overall, fasting had little effect, and the maximal activity of cathepsins in pancreas of fasted rats was in the lysosome-enriched fraction L — same as that in normally fed rats (Figure 7A). In contrast, both CR and Arg pancreatitis caused a dramatic decrease in CatL and CatB activities in fraction L, so that the maximal activity shifted to the heavier, ZG-enriched fraction Z (Figure 7A). This was accompanied by a moderate increase in activities of cathepsins in fraction Z (see Figure 7, A and B).

For CatB, a similar shift in maximal activity from fraction L to Z was previously reported in CR model (30, 36) and interpreted as redistribution (missorting) of CatB to the ZG-containing fraction. However, changes in cathepsin activity in a given fraction could result from changes in either its level or the enzyme's "molecular" activity. Our immunoblot data showed that pancreatitis did not cause any significant redistribution of CatB from fraction L to Z (Figure 6D), arguing against missorting of CatB to the ZG-containing fraction. Therefore, we next examined whether pancreatitis affected "molecular activity" of CatB and/or CatL.

Pancreatitis inhibits molecular activity of CatL in fractions containing autophagic vacuoles. For this analysis (see details in Methods), we examined whether the changes in activities of cathepsins in the subcellular fractions (Figure 7A) could be accounted for by changes in the levels of their active (processed) forms, assessed by immunoblot (Figure 6). We observed that CatL and CatB activities in the lysosome-enriched fraction L had a several-fold

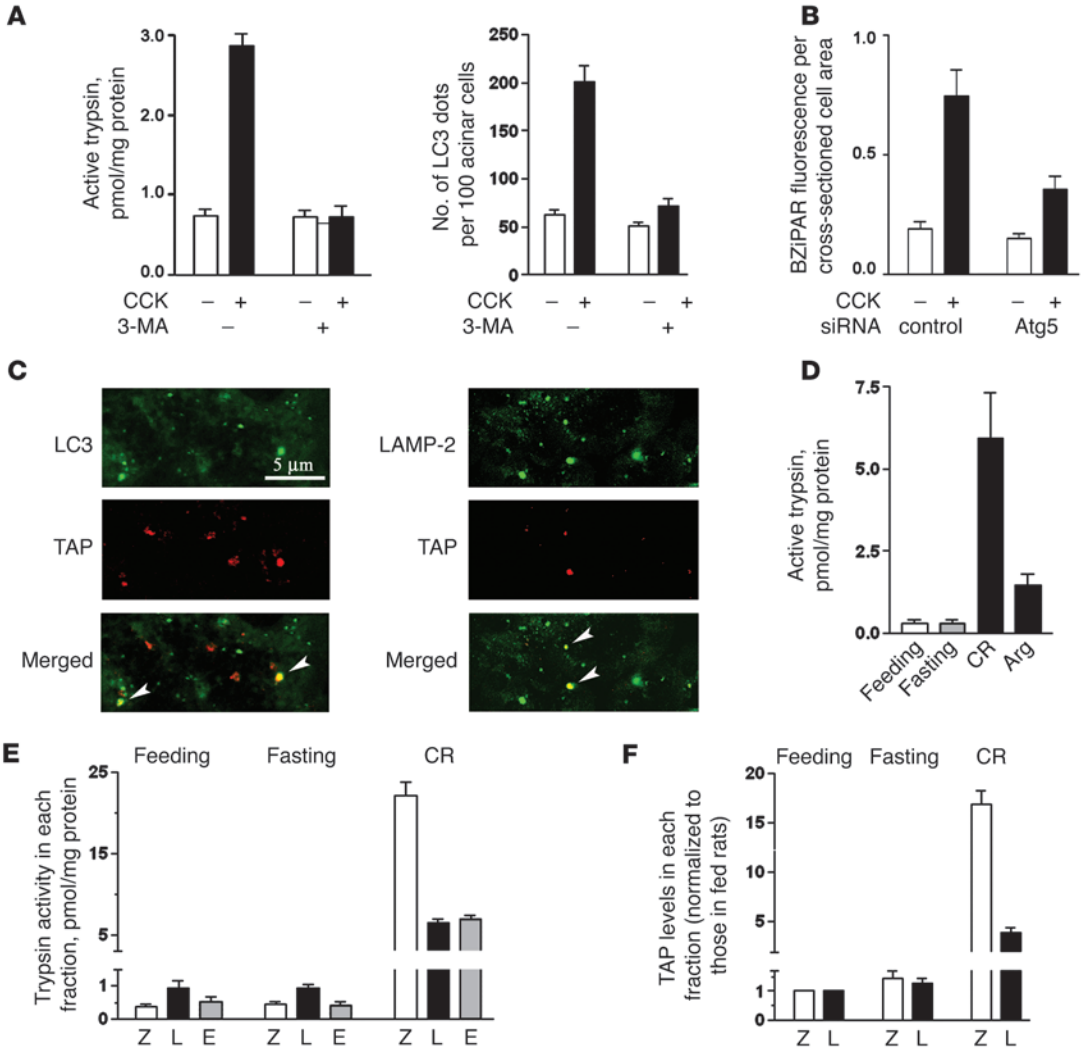

Figure 8

Autophagy impairment mediates intra-acinar trypsin accumulation in pancreatitis. (**A**) Rat pancreatic acinar cells were incubated with or without 100 nM CCK and 10 mM 3-MA. Trypsin activity after 30-minute incubation was measured in cell homogenates by a fluorogenic assay. LC3 dots were visualized, as illustrated in Figure 2B, and counted using ImageJ software. (**B**) Mouse acinar cells were transfected with Atg5 siRNA or control siRNA, as described in Methods. The transfection efficiency is illustrated in Figure 1F. Trypsin activity was measured under fluorescence microscope in live cells loaded with a trypsin substrate BZiPAR and incubated for 30 minutes with and without 100 nM CCK (see Supplemental Figure 6). The fluorescence from cleaved BZiPAR was measured per cross-sectioned cell area using ImageJ software, and 150–200 acinar cells were assessed for each condition. (**C**) Rats were subjected to CR pancreatitis and killed 30 minutes after the first CR injection. Pancreatic tissue sections were double immunostained for LC3 and TAP or LAMP-2 and TAP (colocalization shown by arrowheads). (**D**–**F**) Rats were subjected to fasting and CR or Arg pancreatitis (see Methods), and pancreatic subcellular fractions were obtained as in Figure 4. (**D** and **E**) Trypsin activity was measured in whole tissue homogenates or subcellular fractions by a fluorogenic assay. (**F**) TAP levels in fractions Z and L were measured by ELISA and in each fraction were normalized to those for the feeding conditions. Values in **A**, **B**, and **D**–**F** are mean ± SEM (n = 3).

decrease in pancreatitis, but there was little decrease in the total amount of their active forms in this fraction. This implies that pancreatitis causes an inhibition of CatL and CatB molecular activity in fraction L.

The effect of pancreatitis on the molecular activity of cathepsins in the ZG-enriched fraction Z was less clear, as the models of pancreatitis displayed increases in both the activity (per mg protein) and the amount of processed cathepsin forms in this fraction (Figure 7B). For CatL, the increases in activity in fraction Z (up to ~2-fold increases compared with feeding conditions) were much smaller than the 4- to 6-fold increases in the amount of its active forms in this fraction (Figure 7B). These results indicate that pancreatitis partially inactivates CatL in fraction Z. The increase in CatB activity in fraction Z was comparable with CatL. However, in contrast with CatL, it was not accompanied by any significant increase in the amount of CatB active forms in fraction Z (Figure 7B). This suggests that pancreatitis may stimulate CatB molecular activity in fraction Z.

With respect to the analysis in Figure 7B, we make no assumption as to whether the partially processed (e.g., single-chain)

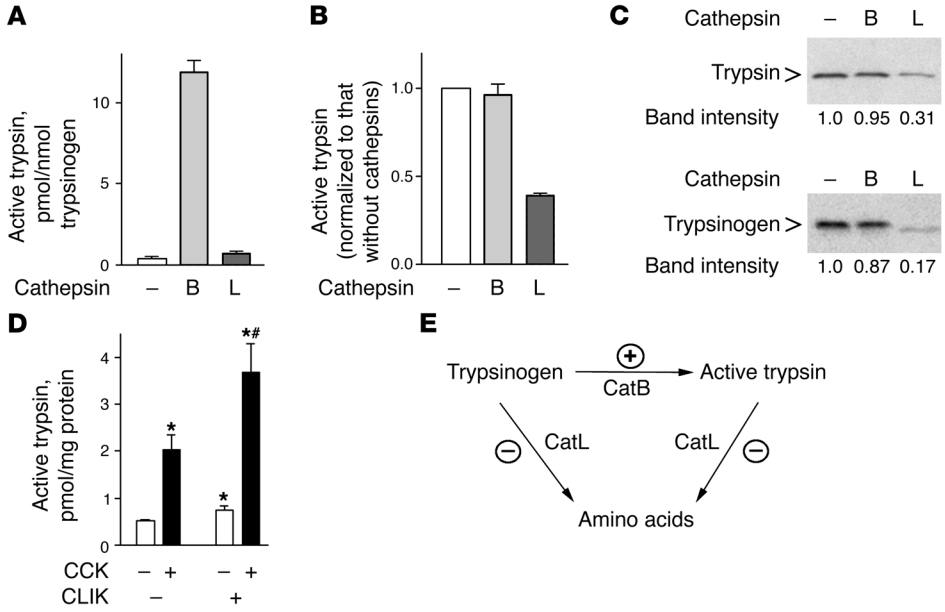

Figure 9

CatL but not CatB inhibits trypsin activity by degrading both trypsin and trypsinogen. (**A**–**C**) Effects of CatB and CatL on trypsinogen activation and degradation in cell-free system. Trypsinogen (**A**) or trypsin (**B**) was incubated for 2 hours with and without CatB or CatL, as described in Methods, and trypsin activity was measured by a fluorogenic assay. (**C**). Levels of trypsinogen and trypsin remaining after the 2-hour incubation with CatB or CatL were measured by immunoblot. (**D**) Rat pancreatic acinar cells were incubated for 30 minutes with and without 100 nM CCK, in the presence and absence of the specific CatL inhibitor CLIK-148 (20 mM). Trypsin activity was measured by a fluorogenic assay. Values in **A**, **B**, and **D** are mean ± SEM (n = 3). $^{*}P < 0.05$ versus control cells; $^{\#}P < 0.05$ versus CCK alone. (**E**). Schematic illustrating the hypothesis that the pathological, intra-acinar trypsin accumulation results from an imbalance between the activities of CatB, which converts trypsinogen to trypsin, and CatL, which degrades both trypsin and trypsinogen. The stimulatory and inhibitory effects of pancreatitis on these enzymes are shown by (+) and (–) symbols, respectively.

cathepsin form is more or less active than its fully mature, double-chain form. The available data (9, 46) indicate that the "molecular activities" of single-chain cathepsin forms may be the same or even higher than of their double-chain forms.

In contrast to pancreatitis, fasting had no major effect on the "molecular activities" of CatL and CatB, compared with feeding conditions. In particular, the fasting-induced moderate increases in CatB and CatL activities in fraction Z were proportional to the levels of the active (processed) forms of cathepsins (Figure 7B).

Together, the results show that pancreatitis causes a pronounced decrease in the activity of CatL and CatB in the lysosome-enriched fraction L. Our analysis also indicates that pancreatitis inhibits CatL molecular activity in both fractions (Z and L) containing autophagic vacuoles. Inhibition of CatL activity may represent a key mechanism underlying pancreatitis-induced inhibition of lysosomal protein clearance and retardation of autophagic flux. Different from CatL, pancreatitis inhibits the molecular activity of CatB in fraction L but likely increases it in fraction Z.

Cathepsin inhibition promotes acinar cell vacuolation. Incubations of rat pancreatic acinar cells with E-64d (a potent inhibitor of both CatB and CatL), CA-074me (a specific inhibitor of CatB), or CLIK-148 (a specific inhibitor of CatL) (47) all caused a dramatic increase in the cross-sectional area occupied by vacuoles (Supplemental Figure 5). Interestingly, the vacuoles induced by E-64d were smaller than those induced by inhibition of each cathepsin alone (Supplemental Figure 5A). Correspondingly, the number of vacuoles increased to a greater extent with E-64d than with the selective inhibitors of CatB or CatL (Supplemental Figure 5C). The reason for these morphologic differences remains to be explored, but the observations suggest that inhibition of lysosomal hydrolases alone can cause acinar cell vacuolation.

Autophagy impairment mediates the pathological, intra-acinar accumulation of trypsin in pancreatitis

Impaired autophagy mediates intra-acinar trypsinogen activation. As stated above, the current paradigm for trypsinogen activation (19, 22, 23) is that it is caused by CatB missorting, leading to its redistribution to ZG-containing compartment(s). Our immunoblot data, however, did not show redistribution of active CatB. Alternatively, we hypothesized that there is a link between autophagy impairment in pancreatitis and the intra-acinar trypsinogen activation.

Blocking autophagy induction with 3-MA completely prevented trypsinogen activation induced by CCK hyperstimulation of mouse pancreatic acinar cells (Figure 8A). (By counting LC3 dots in acinar cells, we confirmed that 3-MA in these experiments indeed blocked the CCK-induced autophagy [Figure 8A].) Further, siRNA knockdown of Atg5, a key mediator of autophagy induction (2, 28), inhibited CCK-induced trypsinogen activation (Figure 8B and Supplemental Figure 6) to the same extent as it inhibited Atg5 expression (Figure 1F, inset). A similar inhibition of trypsinogen activation has been recently reported (25) in pancreatic acinar cells isolated from *Atg5*-deficient mice.

In this context, we noticed that a number of dissimilar compounds that have been shown to inhibit trypsinogen activation in models of acute pancreatitis share a common feature — they all inhibit autophagy but act through different mechanisms. These

include the PI3-kinase inhibitors LY294002 and wortmannin (48, 49) and the cytosolic Ca^{2+} chelators BAPTA/EGTA (50, 51), which all block autophagy induction (2, 3, 52), and bafilomycin, monensin, and chloroquine (53), which dissipate pH gradients and thus block the fusion of lysosomes with autophagosomes (54). We confirmed that all these compounds blocked trypsinogen activation induced by CCK hyperstimulation in isolated rat pancreatic acinar cells (data not shown).

The immunofluorescence data indicated autophagic vacuoles make up one compartment, in which trypsinogen activation occurs in pancreatitis (Figure 8C). Both the autophagic marker LC3-II and the lysosomal marker LAMP-2 partly colocalized with trypsinogen activation peptide (TAP; an oligopeptide cleaved off trypsinogen in the process of its conversion to active trypsin).

In contrast to that found in pancreatitis, there was no trypsinogen activation in pancreas of rats fasted even for a long time, up to 64 hours (Figure 8D and Supplemental Figure 7). Similarly, there was no trypsinogen activation in pancreas of mice fasted for 24 hours (data not shown), a condition that greatly activates autophagy in the exocrine pancreas (28). Further, we observed that induction of autophagy with rapamycin, an inhibitor of mTOR (kinase that blocks initial stages of autophagy [refs. 2, 3]), increased neither the basal trypsin activity nor the CCK-induced trypsinogen activation in rat acinar cells (data not shown). These results indicate that autophagy activation by itself does not induce trypsinogen activation.

The distribution of trypsin activity in rat pancreatic subcellular fractions was very different for pancreatitis and fasting (Figure 8E). In pancreas of fasted rats, the maximal trypsin activity was in the lysosome-enriched fraction L (the same as in normally fed rats), and the levels of active trypsin in all fractions did not change, compared with feeding conditions. In CR pancreatitis, trypsin activity in fraction L had an approximately 5-fold increase, but it was induced more than 40 fold in the ZG-enriched fraction Z (Figure 8E). Similar results were obtained with respect to TAP (Figure 8F): while fasting had no significant effect, CR pancreatitis caused TAP accumulation in fraction Z to a much greater extent than in fraction L.

The data in Figure 8 and Supplemental Figure 7 show that fasting does not induce the pathological, intra-acinar trypsinogen activation, a hallmark of pancreatitis. On the other hand, the results with autophagy inhibitors or Atg5 inactivation (as well as ref. 25) indicate that autophagy is necessary for trypsinogen activation in acinar cells. Taken together, these findings strongly suggest that it is impaired autophagic function, but not autophagy activation per se, that mediates the pathological, intra-acinar accumulation of trypsin. Indeed, the observed increase in active trypsin in fraction Z can be explained by accumulation of "heavy", ZG-containing autophagic vacuoles due to retarded autophagic flux in pancreatitis. Because our results implicated CatL inhibition as a mechanism underlying the defective protein clearance in pancreatitis, we further hypothesized that CatL dysregulation is involved in the intra-acinar accumulation of trypsin.

CatL but not CatB degrades trypsin. To assess CatL involvement in trypsinogen activation, we first compared the effects of CatB and CatL on the trypsinogen conversion to trypsin, as well as the proteolytic degradation of trypsin and trypsinogen, in a cell-free system. In these experiments (Figure 9, A–C), we used the same amount of activity units for CatL and CatB with trypsin or trypsinogen as substrates. CatB efficiently converted trypsinogen to active trypsin (Figure 9A), as previously reported (19, 38, 39). At the same time, CatB neither inhibited the activity of recombinant trypsin (Figure 9B) nor caused any significant degradation of trypsin or trypsinogen (Figure 9C). The effects of CatL were exactly opposite (Figure 9, A–C). CatL did not convert trypsinogen into trypsin (even at 5 times greater concentration; data not shown), but it efficiently degraded both trypsin and trypsinogen and markedly decreased trypsin activity. These findings are in accordance with preliminary reports by Lerch, Halangk, and colleagues (40–42), which indicate that CatL can degrade trypsin and trypsinogen.

We next measured the effects of a specific CatL inhibitor, CLIK-148 (which does not affect CatB [ref. 47]), on trypsinogen activation in CCK-hyperstimulated acinar cells. CLIK-148 significantly increased both the basal and CCK-induced trypsin activity (Figure 9D), indicating that CatL negatively regulates trypsinogen activation in acinar cells.

Based on these findings, we propose that the pathological, intra-acinar accumulation of trypsin in pancreatitis is caused by an imbalance between the enhanced CatB-mediated trypsinogen conversion to trypsin and the inefficient degradation of trypsin and trypsinogen by CatL. This hypothesis is illustrated in the schematic in Figure 9E.

Discussion

To examine the role of autophagy in acute pancreatitis, this study compared autophagic responses in in vivo and in vitro experimental models of pancreatitis with the physiological autophagy induced by fasting. Our findings revealed striking differences in autophagy characteristics between the 2 conditions, which led us to conclude that autophagy is impaired in acute pancreatitis. (a) Pancreatitis caused accumulation in acinar cells of large vacuoles (many-fold larger than in fasted animals), containing partially degraded material. Accumulation of such vacuoles is a manifestation of retarded progression/resolution of autophagy (3). (b) Autophagic protein degradation was markedly inhibited in the in vitro model of pancreatitis. (c) Further evidence for retarded autophagic flux was the dramatic accumulation of lysosomal markers Rab7 and LAMPs in the heavier, ZG-enriched fraction that we found in both CR and Arg pancreatitis. This observation is consistent with accumulation of heavy autolysosomes (containing incompletely degraded material) due to inefficient lysosomal clearance. In contrast, fasting did not affect the subcellular distribution of lysosomal markers. (d) Finally, we found that processing/maturation of CatL and CatB is impaired in pancreatitis but not with fasting.

We considered 2 mechanisms that might underlie autophagic flux impairment in pancreatitis. One possibility could be the blockade of autophagosome fusion with lysosomes, which occurs in lysosomal diseases (10). However, the presence of a great number of vacuoles with partially degraded material in pancreas of animals with pancreatitis as well as in human tissue argues against this possibility. Indeed, we found that colocalization of the lysosomal markers Rab7 and LAMP-2 with the autophagic marker LC3-II increased in models of pancreatitis, which would not occur if autolysosome formation were blocked. The increased colocalization, however, is consistent with retarded autophagy progression.

Another mechanism for the impaired autophagic flux in pancreatitis is a decreased activity of lysosomal hydrolases, resulting in inefficient lysosomal clearance. Evidence to support this mechanism is provided by our finding that processing/maturation of CatL and CatB is defective in pancreatitis. For both cathepsins,

pancreatitis caused a shift from fully processed, double-chain form toward immature, single-chain form. The effect was most pronounced for CatL, resulting in the appearance of its immature form. The impaired cathepsin processing was associated with a dramatic decrease in CatL and CatB activities in the lysosome-enriched fraction L in both CR and Arg pancreatitis. By contrast, fasting did not cause any abnormal cathepsin processing, and the maximal activities of both CatL and CatB remained in fraction L, same as in normal pancreas.

Pancreatitis affected the levels of cathepsins in the pancreatic tissue subcellular fractions. The effect was more dramatic for CatL, resulting in accumulation of its active (processed) forms in the ZG-enriched fraction Z. In contrast, there was no redistribution of CatB protein (as shown using Western blot) from fraction L to Z, in either CR or Arg pancreatitis. By combining the measurements of protein levels and activities of cathepsins, we further showed that the molecular activity of CatL was reduced in both fractions L and Z, i.e., the fractions containing autophagic vacuoles. Differently, our analysis indicated that the molecular activity of CatB was inhibited in fraction L but might be increased in fraction Z.

The differences in the effect of pancreatitis on CatL and CatB processing and subcellular distribution may be related to the known differences in endolysosomal traffic and maturation of these cathepsins (5). As a rule, active CatL exists as its fully mature, double-chain form in lysosomes, whereas active CatB is present as both single- and double-chain forms and localizes to not only lysosomes but also prelysosomal structures (5). Thus, the greater effect of pancreatitis on CatL, compared with that on CatB, might indicate that pancreatitis affects lysosomes more than prelysosomal structures.

Taken together, the results suggest that defective cathepsin processing and activities may underlie the inefficient protein degradation and retarded autophagy progression in pancreatitis. The mechanism(s) responsible for the defective cathepsin processing and activities in pancreatitis remain to be established.

Our results indicate that impaired autophagy mediates 2 key pathological events of pancreatitis: acinar cell vacuolation and intra-acinar trypsin accumulation. Acinar cell vacuolation is a long noted but poorly understood manifestation of pancreatitis. Studies from decades ago (14–17) used terms such as "autophagic vacuoles"; however, both the identity of these vacuoles and the mechanisms triggering their formation have not been established. Our data show that blocking autophagy with 3-MA or Atg5 inactivation greatly inhibits vacuolation of acinar cells, thus indicating that autophagic vacuoles are indeed a major type of vacuoles in pancreatitis. These results corroborate the recent study (25), which showed that Atg5-knockout mice displayed a marked decrease in acinar cell vacuolation in the CR model. However, that study did not consider autophagy impairment but instead concluded that acinar cell vacuolation is caused by "excessive" autophagy activation in pancreatitis. This conclusion was based on the observed increases in the level of LC3-II and the number of LC3-positive vacuoles (25). The pancreatitis models we studied also displayed increases in LC3-II levels and the number of LC3-positive vacuoles. However, as shown in many publications (26), these parameters cannot be used as a measure of autophagy activation, as such increases may result from either autophagy activation or its impairment. It is also worth noting that when autophagy progression/resolution is impaired its activation becomes "excessive."

The comparison with the physiological autophagy response induced by fasting indicates that it is not autophagy activation per se but its impairment (and in particular, the defective cathepsin processing) that is responsible for the pathological manifestations of acute pancreatitis. Indeed, we show that inhibition of both CatB and CatL causes a dramatic increase in vacuoles in acinar cells. In fact, pharmacologic or genetic inactivation of cathepsins has been shown in other cells to block autophagy progression, resulting in accumulation of autophagic vacuoles (3, 47, 55). The broad-spectrum cathepsin inhibitor, leupeptin, caused accumulation of large autophagic vacuoles in pancreatic acinar cells (56).

For many years, the only established mechanism underlying intra-acinar accumulation of active trypsin in pancreatitis has been an increase in trypsinogen conversion to trypsin by CatB (38, 39). The current "colocalization hypothesis," proposed by Steer and Saluja (19, 22, 23), postulates that this increase is caused by defective segregation ("missorting") of CatB, which leads to its redistribution into ZG-containing compartment(s). Thus, colocalization of CatB with trypsinogen is proposed to be a key initiating event of pancreatitis (19, 21, 22). Of note, redistribution of CatB into ZG-containing fraction Z was inferred from changes in CatB activity in the subcellular fractions (30, 36) and not from direct measurement of CatB protein levels in models of pancreatitis. The colocalization hypothesis received criticism, in part because a significant CatB activity in fraction Z is also observed in normal pancreas (20, 21, 36, 57).

Importantly, our immunoblot data show no redistribution of CatB into the ZG-enriched fraction Z in pancreatitis and indicate that the observed changes in CatB activity result from its' abnormal processing. These findings argue against the colocalization hypothesis. Alternatively, we propose that in the normal process of autophagy, ZGs undergo autophagic degradation, and thus a part of them become sequestered in autophagic vacuoles, as evidenced by EM (28) and colocalization of amylase with LC3-II (see Results). This is the site in which CatB "meets" and activates trypsinogen, resulting in the low basal trypsin activity in normal pancreas. Hence, colocalization of cathepsins with ZG is itself not pathological. In physiological autophagy (i.e., fasting), this colocalization does not lead to excessive accumulation of active trypsin, because trypsinogen activation is balanced by efficient lysosomal degradation of sequestered ZG content. By contrast, in pancreatitis, trypsin accumulates in acinar cells due to deficient autophagic protein degradation.

Our hypothesis explains the findings in the present study and ref. 25 that autophagy inhibition by pharmacologic, molecular, and genetic means abrogated trypsinogen activation in acinar cells, which demonstrated the involvement of autophagy. We further detected TAP colocalization with LC3-II and LAMP-2 in CR pancreatitis, indicating autophagic vacuoles as one site of the intra-acinar cell trypsinogen activation. The finding in our study that pancreatitis induces accumulation of multiple lysosomal markers (not only cathepsins but also Rab7 and LAMPs) in the ZG-enriched fraction Z is difficult to explain by cathepsin missorting.

Our results suggest that trypsin accumulates in acinar cells due to disturbed equilibrium between its generation from trypsinogen, mediated by CatB, and the degradation of trypsin and trypsinogen by CatL (and possibly, other cathepsins). According to our hypothesis, such imbalance is caused by defective processing and activities of cathepsins in pancreatitis and not by "excessive" autophagy activation, as suggested in ref. 25. Indeed, our data show that physiological autophagy does not lead to intra-pancreatic accumulation of active trypsin, even with prolonged fasting.

In sum, we provide evidence that acute pancreatitis causes profound autophagy impairment, which is responsible for 2 key manifestations of this disease: the accumulation of large vacuoles in acinar cells and the intra-acinar trypsinogen activation. Specifically, our findings indicate that pancreatitis causes inefficient protein clearance, leading to retarded progression (a "traffic jam") from autophagosomes to autolysosomes. The results suggest that one mechanism mediating autophagic flux retardation in pancreatitis is the impaired processing and activity of cathepsins. Furthermore, autophagy impairment may be a manifestation of a more general phenomenon, indicating that the endolysosomal traffic is disordered in acute pancreatitis. Indeed, trypsinogen activation has been recently reported (51) in endocytic vacuoles in response to CCK hyperstimulation of acinar cells. A number of characteristics of pancreatitis are similar to those observed in lysosomal disorders (which are mostly caused by mutations that inactivate lysosomal hydrolases or affect their delivery to lysosomes) — such as block of autophagy, impaired maturation of cathepsins, decreased protein degradation, cell vacuolation and death, and the inflammatory response (10). Thus, our findings indicate that acute pancreatitis has features of a lysosomal disease, which should be taken into consideration in designing strategies to treat or mitigate pancreatitis.

Methods

Reagents. Antibodies against LC3, LAMP-1, Beclin1, and CatB were from Santa Cruz Biotechnology Inc.; antibody against LAMP-2 was from Sigma-Aldrich; antibodies against Rab7, Atg5, and p44/42 MAP kinase (ERK1/2) were from Cell Signaling Technology; antibody against EEA1 was from BD Biosciences; antibody against COX IV was from Molecular Probes; antibody against trypsinogen was from Chemicon–Millipore; antibody against PDI was from Stressgen. The antibody against CatL was developed by A.H. Erickson. CCK was from American Peptide; CR was from Peninsula Laboratories; Arg was from Sigma-Aldrich; liver CatB (0.25 units/mg protein) and CatL (1 unit/mg protein) were from Calbiochem; bovine pancreas trypsinogen was from Sigma-Aldrich; recombinant trypsin was from Roche; BZiPAR [rhodamine 110 bis-(CBZ-L-isoleucyl-L-prolyl-arginine amide) dihydrochloride] was from Molecular Probes. CatB inhibitor CA-074me was from Calbiochem; the selective CatL inhibitor CLIK-148 was developed by N. Katunuma. Fluorogenic substrates for CatB (Z-Arg-Arg-AMC) and CatL (Z-Phe-Arg-AMC) were from Calbiochem; trypsin specific substrate, Boc-Gln-Ala-Arg-AMC, was from Biomol International. All other reagents were from Sigma-Aldrich.

Experimental pancreatitis. Cerulein pancreatitis was induced as described (31), in male (200–250 g) Sprague-Dawley rats and in CD-1 or transgenic GFP-LC3 (28) mice (25–30 g) (a gift from N. Mizushima, Tokyo Medical and Dental University, Tokyo, Japan, and RIKEN BioResourse Center, Koyadai, Japan. Rats received 4 and mice received 7 hourly i.p. injections of 50 μg/kg CR. Control animals received similar injections of physiological saline. The animals were fasted overnight (for 17 hours). Arginine pancreatitis was induced in rats as described (31), with 2 hourly i.p. injections of 2.5 g/kg Arg; controls received similar injections of saline. In this model, rats were not fasted and were sacrificed 24 hours after the first injection. CDE pancreatitis (58) was induced in young (14–15 g) female CD-1 mice fed either CDE or control diet. Fresh aliquots of the diets were provided every 12 hours, and the food intake was measured. Mice were sacrificed 48 or 72 hours after initiation of the diet.

Animals were euthanized by CO_2-induced asphyxiation, and the blood and pancreas were harvested for measurements. The development of pancreatitis was confirmed by histological changes and by increased levels of amylase and lipase in serum, as measured in a Hitachi 707 analyzer (Antech Diagnostics). The experimental protocols were approved by the animal research committee of the Veterans Affairs Greater Los Angeles Healthcare System, in accordance with the NIH guidelines.

Fasting. In fasting experiments, we took into account the nocturnal eating habits of rodents. It has been shown, for example, that the number and size of ZGs in exocrine pancreas (59) and the amylase content in the functionally similar parotid gland (60) all increase during the day and then markedly decrease during the nocturnal feeding period. Thus, for normally fed controls, we used animals sacrificed at 5 PM, that is, prior to start of the nocturnal feeding period. Fasting animals were deprived of food (laboratory chow) overnight and euthanized either at 10 AM next day (after 17 hours fasting) or 5 PM (after 24 hours fasting). These fasting times encompass the duration of CR pancreatitis experiments. In some experiments, rats were deprived of food for longer times, up to 64 hours.

Isolation of pancreatic acinar cells. Isolation of cells from rats or mice was performed using a collagenase digestion procedure as described (31, 49, 61). Dispersed pancreatic acini were then incubated at 37°C in 199 medium in the presence or absence of CCK and other agents as indicated.

Prolonged culture of acinar cells. Mouse pancreatic acinar cells, isolated using standard collagenase digestion procedure (31, 49, 61), were cultured (for up to 3 days) according to ref. 32, on collagen IV in DMEM medium containing 15% FBS, 5 ng/ml EGF, 0.25 μg/ml amphotericin B, 0.5 mM IBMX, 0.2 mg/ml soybean trypsin inhibitor, 100 U/ml penicillin, and 100 μg/ml streptomycin. We used the prolonged (24-hour) acinar cell culture for transfections and measurement of long-lived protein degradation (see below). As shown in Supplemental Figure 8, these cells retained acinar cell phenotype and functional responses. In particular, they released amylase upon CCK stimulation and, moreover, retained the hallmark biphasic response curve that displays inhibited amylase release at supramaximal CCK concentrations (Supplemental Figure 8D). Further, the supramaximal CCK induced trypsinogen activation in cultured acinar cells (Supplemental Figure 8E) to a similar extent as that in freshly isolated cells.

The prolonged culture caused some damage in acinar cells. For example, after 24-hour culture, vacuoles (assessed on cell sections stained with toluidine blue) occupied 1.6% ± 0.4% of cross-sectional cell area, compared with 0.7% ± 0.2% of cross-sectional cell area in freshly isolated mouse acinar cells. Only the number, but not the average size of vacuoles in acinar cells, increased during culture (both measured with the use of ImageJ software; http://rsbweb.nih.gov/ij/). Necrosis (measured by trypan blue exclusion) increased to 12% ± 3% after 24-hour culture, compared with 4% ± 2% necrosis in freshly isolated mouse acinar cells. (Values are means ± SEM from 100–150 acinar cells in at least 3 separate acinar cell preparations.)

Transfections. Acinar cells in prolonged culture (see above) were transfected with Atg5 siRNA by using ON-TARGETplus SMARTpool from Dharmacon, consisting of equal amounts of 4 RNA duplexes targeting the gene of interest (i.e., *Atg5*). The Atg5 siRNA sequences (given as sense/antisense pairs) were as follows: GCAUAAAAGUCAAGUGAUCUU/5′-GAUCACUUGACUUUUAUGCUU; CCAAUUGGUUUACUAUUUGUU/5′-CAAAUAGUAAACCAAUUGGUU; CGAAUUCCAACUUGCUUUAUU/5′-UAAAGCAAGUUGGAAUUCGUU; and UUAGUGAGAUAUGGUUUGAUU/5′-UCAAACCAUAUCUCACUAAUU. For negative control, we used si*CONTROL* Non-Targeting pool; for positive control, we used the si*GLO* Cyclophilin B siRNA, labeled with fluorescent DY547 (all from Dharmacon). Transfections (100 pmoles of each siRNA) were performed using the Amaxa Nucleofactor electroporation system (Amaxa Transfection). The transfection efficiency, assessed by using si*GLO* cyclophilin B siRNA (Supplemental Figures 6 and 8), was 50%–70%. Transfected cells preserved acinar cell phenotype (Supplemental Figure 8) and responded to CCK with increases in vacuoles (Figure 1F) and trypsinogen activation (Figure 8B and Supplemental Figure 6).

The electroporation procedure, using the Amaxa Nucleofactor system, increased necrosis to 30% ± 8% (as measured by trypan blue exclusion), compared with 12% ± 3% in nontransfected acinar cells after 24-hour culture. This increase was due to electroporation and not transfection per se. Importantly, the extent of necrosis was the same in cells transfected with control and Atg5 siRNA. Also, there was no effect of transfections on acinar cell vacuolation. Of note, all the measurements on transfected cells were performed under the microscope, in cells with an intact plasma membrane.

Subcellular fractionation. Subcellular fractionation of pancreatic tissue was performed by differential centrifugation as described by Saluja and colleagues (30, 36). The dissected pancreas was homogenized in 8 ml of homogenization buffer with 5 full strokes, and the nuclei and cell debris were sedimented at 150 *g*. The postnuclear supernatant was centrifuged at 1,300 *g*, and the pellet collected was referred to as fraction Z (see Results). The supernatant was further centrifuged at 12,000 *g*, and both the 12,000-*g* pellet (fraction L) and supernatant (fraction E) were collected. Total protein in the fractions was measured by Bradford assay (Bio-Rad). Of note, fractions Z and L contained essentially the same amount of total protein, whereas this was approximately 4 times greater in fraction E. The amounts of total protein in the fractions were consistent across experimental conditions.

EM. For EM, the tissue (cut into 1-mm cubes) or the pellets from the subcellular fractions were fixed at 4°C in 2.5% glutaraldehyde in 0.15 M sodium cacodylate (pH 7.4) overnight. After postfixation in 1% OsO_4, followed by uranyl acetate, tissue was dehydrated in ethanol and embedded in epoxy resin. Then, 100-nm-thick sections were stained with uranyl acetate and examined in a Hitachi-600 electron microscope. For quantification, the areas of each autophagic vacuole and nucleus were measured on each print, and the average size of autophagic vacuoles was normalized to that of the nuclei in the same electron micrograph.

Immunogold EM. For immunogold labeling, pancreata from GFP-LC3 transgenic mice (28) were fixed in 4% buffered formaldehyde (pH 7.2). The tissue pieces were then either embedded in LR White resin using a microwave-assisted protocol (62) or were cryoprotected in dimethyl formamide, frozen in liquid propane, freeze substituted in dry acetone containing 1% OsO_4, and embedded in Lowicryl HM20. The embedded tissues were sectioned, mounted onto metal specimen grids, and immunolabeled by using goat anti-LC3 antibodies. Sections were visualized using a bridging, unconjugated rabbit anti-goat antibody followed by 10 nm protein A-gold (University of Utrecht, Utrecht, The Netherlands). Sections were stained with uranyl acetate and lead citrate to enhance contrast.

Light microscopy. For histological evaluation (31), pancreatic tissue was fixed in 10% buffered formaldehyde, embedded in paraffin, sectioned, and stained with H&E. Images were captured with a Nikon Eclipse TE2000-S microscope equipped with a CCD camera, using the SPOT imaging software (Diagnostic Instruments). The number of vacuoles and the percentage of cross-sectioned cell area occupied by vacuoles on pancreatic tissue sections were quantified using MetaMorph 6.1 software. The number of vacuoles in isolated acinar cells was quantified on cells stained with toluidine blue as described in ref. 63. H&E images of pancreatic tissue from patients with acute pancreatitis were provided by D.S. Longnecker.

Immunofluorescence. For immunolabeling, pancreas was dissected and fixed for 2 hours in 4% paraformaldehyde, and tissue pieces were equilibrated for 2 hours at 4°C in a 15% sucrose-phosphate buffer solution and then embedded in OCT compound (Miles). Then, 5-μm frozen pancreatic tissue sections were fixed in 0.1 M phosphate buffer containing 4% paraformaldehyde, washed several times in PBS supplemented with 0.5% saponin and 0.2% Tween-20, and blocked with 2% donkey serum. Tissue sections then incubated overnight with primary antibody, followed by incubation with secondary antibody conjugated with FITC or Texas Red (Jackson ImmunoResearch Laboratories). A different procedure (64) was applied for TAP immunolabeling.

Images were acquired with a Zeiss LSM 510 confocal microscope using a ×63 objective. To determine the percentage colocalization of 2 proteins, images obtained with the use of corresponding antibodies were loaded into ImageJ software (http://rsbweb.nih.gov/ij/) and the ratios of green (FITC) or red (Texas Red) cells to merged cells were determined with the colocalization plug-in.

Measurement of the rate of long-lived protein degradation. The long-lived protein degradation rate was measured as described by Mizushima and Mortimore and colleagues (27, 65). Mouse pancreatic acinar cells, isolated using standard collagenase digestion procedure (31, 49, 61), were first cultured for 6 hours as specified above (see *Prolonged culture of acinar cells*), on collagen IV in DMEM medium supplemented with [^{14}C]-valine (4 mCi/mmol specific activity); washed by centrifugation to remove unincorporated radioisotope and the released amino acids; and then the cells were replated on collagen IV and chased for 16 hours in fresh DMEM medium containing 2 mM cold valine, during which time all short-lived proteins were degraded (65, 66). After that, cells were washed 3 times by centrifugation in 199 medium containing 2 mM cold valine and further incubated on plastic for 4 hours in either 199 medium (i.e., containing amino acids) with or without CCK (as indicated in Figure 3) or "nutrient-free" medium devoid of amino acids (Sigma-Aldrich), which is used for in vitro starvation experiments.

For each condition, parallel incubations were done with or without the autophagy inhibitor 3-MA (10 mM). The purpose of using 3-MA is to quantify protein degradation by both autophagic and nonautophagic mechanisms (27). The values obtained in the presence of 3-MA were subtracted as the nonautophagic background, producing the net autophagy-mediated rate of long-lived protein degradation. At the end of incubation, protein in both the cells and the incubation medium was precipitated with ice-cold 10% (v/v) trichloroacetic acid (TCA). The soluble radioactivity, which represents degradation products, was separated from intact protein by centrifugation at 12,000 *g* for 10 minutes. The rate of long-lived protein degradation was calculated as the percentage of TCA-soluble radioactivity in both the medium and cells (27).

Measurement of protease activities. Cathepsin activities were measured in pancreatic tissue homogenates and subcellular fractions as described in ref. 67, using fluorogenic substrates specific for CatB (Z-Arg-Arg-AMC) or CatL (Z-Phe-Arg-AMC) (50 μM each). CatB activity was measured in 50 mM phosphate buffer, pH 6.0, and CatL activity was measured in 100 mM sodium acetate buffer, pH 5.5, in the presence of 2 mM EDTA and 2 mM DTT. In measurements of CatL activity, the assay buffer also contained 50 μM CA-074me, a CatB inhibitor.

Trypsin activity was measured in tissue and cell homogenates or subcellular fractions using a specific fluorogenic substrate, Boc-Gln-Ala-Arg-AMC, as described (49, 68). Trypsin activity in live pancreatic acinar cells was measured by using the fluorogenic substrate BZiPAR, as described (69). All solutions for this assay contained 5 μM soybean trypsin inhibitor. Images were obtained in a Nikon Eclipse TE2000-S microscope, and fluorescence quantification was performed using ImageJ software (http://rsbweb.nih.gov/ij/).

TAP measurements. TAP measurements were performed in pancreatic tissue homogenates and subcellular fractions with ELISA (Biotrin International).

Measurements of cathepsin-induced conversion of trypsinogen to trypsin and degradation of trypsin and trypsinogen in cell-free system. Trypsinogen (2 μM) or trypsin (0.2 μM) was incubated for 2 hours at 37°C, with 5 mU CatB or CatL in 0.1 M sodium acetate buffer containing 2 mg/ml BSA and 1 mM EDTA at pH 4.0 or 5.5, respectively. Before use, cathepsins were activated by incubating them on ice for 30 minutes with 1 mM DTT. Enterokinase (0.05 U/μg protein in 0.2 M Tris-HCl, 20 mM $CaCl_2$, pH 7.4) was used as a positive control. We measured both the resulting trypsin activity, by using the fluorogenic Boc-Gln-Ala-Arg-AMC substrate (49, 68), and the levels of trypsinogen and trypsin by immunoblot.

Amylase secretion by isolated acinar cells. Amylase secretion by isolated acinar cells (Supplemental Figure 8D) was measured spectrophotometrically using Phadebas amylase kit (Magle AB), as described previously (49). Values for amylase secretion are ratios between the amount of amylase released into the extracellular medium and the total cellular amylase determined by permeabilizing cells with 1% Triton X-100.

Western blot analysis. Western blot analysis was performed on tissue and cell homogenates or subcellular fractions as described previously (31, 61). Proteins were separated by SDS-PAGE and electrophoretically transferred to nitrocellulose membranes. Nonspecific binding was blocked by 1-hour incubation of the membranes in 5% (w/v) nonfat dry milk or 5% BSA in Tris-buffered saline (pH 7.5). The blots were then incubated for 2 hours or overnight with primary antibodies in the antibody buffer containing 1% (w/v) nonfat dry milk in 0.05% (v/v) Tween 20 in Tris-buffered saline (TTBS), washed 3 times with TTBS, and finally incubated for 1 hour with a peroxidase-labeled secondary antibody in the antibody buffer. The blots were developed for visualization using an enhanced chemiluminescence detection kit (Pierce). Band intensities in the immunoblots were quantified by densitometry using the Scion image analysis software (Scion Co.).

When comparing immunoblots of the whole pancreatic tissue and subcellular fractions, keep in mind that the 3 fractions do not contribute equally to a Western blot of the whole tissue, as the total amount of protein differs among the fractions (see *Subcellular fractionation*). Thus, the tissue immunoblot is not a simple sum of those for individual fractions.

Analysis of the amounts of CatL and CatB active forms in pancreatic subcellular fractions by immunoblot. Two methods were used to assess changes in the active (processed) forms of cathepsins in pancreatic subcellular fractions, based on densitometric intensity of their bands in the immunoblots (see Figure 7B). First, for each sample and for each cathepsin (i.e., CatL or CatB), we calculated the ratio of band intensity of the active forms (single- or double-chain or both together) in a given fraction to the sum of these intensities in all 3 subcellular fractions. The means of these ratios for each condition (e.g., CR pancreatitis or fasting) were further normalized to those for feeding conditions. For example, the mean value for CatB active forms in fraction Z, calculated as the percentage of the total amount of CatB active forms in all 3 fractions, was 34% in CR pancreatitis versus 45% in rats fasted for 17 hours versus 43% in normally fed rats (see Figure 7B). As a second method, we calculated the ratios of band intensity of CatL (or CatB) active forms to its proform in the same subcellular fraction. The mean values for these ratios showed a similar trend of changes; for example, the mean ratio of CatB active forms to its proform in fraction Z was 2.5 in CR pancreatitis versus 3.6 in fasted rats.

Statistics. Results represent means ± SEM from several independent experiments, as specified in figure legends. Differences between 2 groups were analyzed using 2-tailed Student's *t* test. *P* values of less than 0.05 were considered statistically significant.

Acknowledgments

This study was supported by the Department of Veterans Affairs, the NIH grants DK59936 (to A.S. Gukovskaya) and P60 AA11999 (to A.S. Gukovskaya and S.J. Pandol), and, in part, by the American Gastroenterology Association Foundation Designated Research Scholar Award in Pancreatitis (to O.A. Mareninova). The authors thank Noboru Mizushima (Tokyo Medical and Dental University, Tokyo, Japan) and RIKEN BioResourse Center (Koyadai, Japan) for providing the GFP-LC3 transgenic mice and D.S. Longnecker (Dartmouth Medical School, USA) for providing H&E images of pancreatic tissue from patients with acute pancreatitis. The authors also thank the UCLA Microscopic Techniques Core (Marianne Cilluffo) for expert help with immunolabeling, Moses A. Lee for help with Western blot densitometry, and Tina Feng for help with quantification of vacuoles.

Received for publication January 21, 2009, and accepted in revised form July 1, 2009.

Address correspondence to: Anna S. Gukovskaya or Ilya Gukovsky, UCLA/Veterans Affairs Greater Los Angeles Healthcare System, West Los Angeles Veterans Affairs Healthcare Center, 11301 Wilshire Blvd., Blg. 258, Rm. 340, Los Angeles, California 90073, USA. Phone: (310) 478-3711 ext. 41525; Fax: (310) 268-4578; E-mail: agukovsk@ucla.edu (A.S. Gukovskaya). Phone: (310) 478-3711 ext. 41424; Fax: (310) 268-4578; E-mail: igukovsk@ucla.edu (I. Gukovsky).

Portions of this work have appeared in abstract form (2008. *Gastroenterology*. **134**:A428).

1. Mizushima, N., Levine, B., Cuervo, A.M., and Klionsky, D.J. 2008. Autophagy fights disease through cellular self-digestion. *Nature.* **451**:1069–1075.
2. Xie, Z., and Klionsky, D.J. 2007. Autophagosome formation: core machinery and adaptations. *Nat. Cell Biol.* **9**:1102–1109.
3. Levine, B., and Kroemer, G. 2008. Autophagy in the pathogenesis of disease. *Cell.* **132**:27–42.
4. Bohley, P., and Seglen, P.O. 1992. Proteases and proteolysis in the lysosome. *Experientia.* **48**:151–157.
5. Ishidoh, K., and Kominami, E. 2002. Processing and activation of lysosomal proteinases. *Biol. Chem.* **383**:1827–1831.
6. Rowan, A.D., Mason, P., Mach, L., and Mort, J.S. 1992. Rat procathepsin B. Proteolytic processing to the mature form in vitro. *J. Biol.Chem.* **267**:15993–15999.
7. Kominami, E., Tsukahara, T., Hara, K., and Katunuma, N. 1988. Biosyntheses and processing of lysosomal cysteine proteinases in rat macrophages. *FEBS Lett.* **231**:225–228.
8. Erickson, A.H. 1989. Biosynthesis of lysosomal endopeptidases. *J. Cell. Biochem.* **40**:31–41.
9. Brix, K., Dunkhorst, A., Mayer, K., and Jordans, S. 2008. Cysteine cathepsins: cellular roadmap to different functions. *Biochimie.* **90**:194–207.
10. Nixon, R.A., Yang, D.S., and Lee, J.H. 2008. Neurodegenerative lysosomal disorders: a continuum from development to late age. *Autophagy.* **4**:590–599.
11. Saftig, P., Tanaka, Y., Lullmann-Rauch, R., and von Figura, K. 2001. Disease model: LAMP-2 enlightens Danon disease. *Trends Mol. Med.* **7**:37–39.
12. Adler, G., Rohr, G., and Kern, H.F. 1982. Alteration of membrane fusion as a cause of acute pancreatitis in the rat. *Dig. Dis. Sci.* **27**:993–1002.
13. Aho, H.J., Nevalainen, T.J., Havia, V.T., Heinonen, R.J., and Aho, A.J. 1982. Human acute pancreatitis: a light and electron microscopic study. *Acta Pathol. Microbiol. Immunol. Scand. A.* **90**:367–373.
14. Brackett, K.A., Crocket, A., and Joffe, S.N. 1983. Ultrastructure of early development of acute pancreatitis in the rat. *Dig. Dis. Sci.* **28**:74–84.
15. Helin, H., Mero, M., Markkula, H., and Helin, M. 1980. Pancreatic acinar ultrastructure in human acute pancreatitis. *Virchows Arch. A Pathol. Anat. Histol.* **387**:259–270.
16. Koike, H., Steer, M.L., and Meldolesi, J. 1982. Pancreatic effects of ethionine: blockade of exocytosis and appearance of crinophagy and autophagy precede cellular necrosis. *Am. J. Physiol.* **242**:G297–G307.
17. Watanabe, O., Baccino, F.M., Steer, M.L., and Meldolesi, J. 1984. Supramaximal caerulein stimulation and ultrastructure of rat pancreatic acinar cell: early morphological changes during development of experimental pancreatitis. *Am. J. Physiol.* **246**:G457–G467.
18. Niederau, C., and Grendell, J.H. 1988. Intracellular vacuoles in experimental acute pancreatitis in rats and mice are an acidified compartment. *J. Clin. Invest.* **81**:229–236.
19. Steer, M.L. 1999. Early events in acute pancreatitis. *Baillieres Best. Pract. Res. Clin. Gastroenterol.* **13**:213–225.
20. Gorelick, F.S., and Matovcik, L.M. 1995. Lysosomal enzymes and pancreatitis. *Gastroenterology.* **109**:620–625.
21. Halangk, W., and Lerch, M.M. 2005. Early events in acute pancreatitis. *Clin. Lab Med.* **25**:1–15.
22. Saluja, A.K., Lerch, M.M., Phillips, P.A., and Dudeja, V. 2007. Why does pancreatic overstimulation cause pancreatitis? *Annu. Rev. Physiol.* **69**:249–269.
23. Van Acker, G.J., Weiss, E., Steer, M.L., and Perides, G. 2007. Cause-effect relationships between zymogen activation and other early events in secretagogue-induced acute pancreatitis. *Am. J. Physiol. Gastrointest. Liver Physiol.* **292**:G1738–G1746.
24. Sahin-Toth, M. 2006. Biochemical models of hereditary pancreatitis. *Endocrinol. Metab. Clin. North Am.* **35**:303–312, ix.
25. Hashimoto, D., et al. 2008. Involvement of autophagy in trypsinogen activation within the pancreatic

acinar cells. *J. Cell Biol.* **181**:1065–1072.
26. Klionsky, D.J., et al. 2008. Guidelines for the use and interpretation of assays for monitoring autophagy in higher eukaryotes. *Autophagy.* **4**:151–175.
27. Mizushima, N. 2004. Methods for monitoring autophagy. *Int.J. Biochem. Cell Biol.* **36**:2491–2502.
28. Mizushima, N., Yamamoto, A., Matsui, M., Yoshimori, T., and Ohsumi, Y. 2004. In vivo analysis of autophagy in response to nutrient starvation using transgenic mice expressing a fluorescent autophagosome marker. *Mol. Biol. Cell.* **15**:1101–1111.
29. Eskelinen, E.L., Tanaka, Y., and Saftig, P. 2003. At the acidic edge: emerging functions for lysosomal membrane proteins. *Trends Cell Biol.* **13**:137–145.
30. Saluja, A., et al. 1985. In vivo rat pancreatic acinar cell function during supramaximal stimulation with caerulein. *Am. J. Physiol.* **249**:G702–G710.
31. Mareninova, O.A., et al. 2006. Cell death in pancreatitis: caspases protect from necrotizing pancreatitis. *J. Biol. Chem.* **281**:3370–3381.
32. Sphyris, N., Logsdon, C.D., and Harrison, D.J. 2005. Improved retention of zymogen granules in cultured murine pancreatic acinar cells and induction of acinar-ductal transdifferentiation in vitro. *Pancreas.* **30**:148–157.
33. Boya, P., et al. 2005. Inhibition of macroautophagy triggers apoptosis. *Mol. Cell. Biol.* **25**:1025–1040.
34. Hendil, K.B., Lauridsen, A.M., and Seglen, P.O. 1990. Both endocytic and endogenous protein degradation in fibroblasts is stimulated by serum/amino acid deprivation and inhibited by 3-methyladenine. *Biochem. J.* **272**:577–581.
35. Tartakoff, A.M., and Jamieson, J.D. 1974. Subcellular fractionation of the pancreas. *Methods Enzymol.* **31**:41–59.
36. Saluja, A., et al. 1987. Subcellular redistribution of lysosomal enzymes during caerulein-induced pancreatitis. *Am. J. Physiol.* **253**:G508–G516.
37. Bucci, C., Thomsen, P., Nicoziani, P., McCarthy, J., and van Deurs, B. 2000. Rab7: a key to lysosome biogenesis. *Mol. Biol. Cell.* **11**:467–480.
38. Greenbaum, L.M., Hirshkowitz, A., and Shoichet, I. 1959. The activation of trypsinogen by cathepsin B. *J. Biol. Chem.* **234**:2885–2890.
39. Halangk, W., et al. 2000. Role of cathepsin B in intracellular trypsinogen activation and the onset of acute pancreatitis. *J. Clin. Invest.* **106**:773–781.
40. Wartmann, T., Mayerle, J., Ruthenburger, M., Lerch, M.M., and Halangk, W. 2003. Degradation of pancreatic digestive enzymes by Cathepsin L [abstract]. *Pancreatology.* **3**:257–258.
41. Halangk, W., et al. 2003. Cathepsin L in the pancreatic secretory pathway and its effect on disease-relevant trypsinogen mutants [abstract]. *Gastroenterology.* **124**:A585.
42. Halangk, W., et al. 2002. Generation of trypsinogen activation peptide in the exocrine pancreas by different mechanisms [abstract]. *Gastroenterology.* **122**:A93.
43. Kukor, Z., et al. 2002. Presence of cathepsin B in the human pancreatic secretory pathway and its role in trypsinogen activation during hereditary pancreatitis. *J. Biol. Chem.* **277**:21389–21396.
44. Tanaka, Y., Tanaka, R., Kawabata, T., Noguchi, Y., and Himeno, M. 2000. Lysosomal cysteine protease, cathepsin B, is targeted to lysosomes by the mannose 6-phosphate-independent pathway in rat hepatocytes: site-specific phosphorylation in oligosaccharides of the proregion. *J. Biochem.* **128**:39–48.
45. Mach, L., Stuwe, K., Hagen, A., Ballaun, C., and Glossl, J. 1992. Proteolytic processing and glycosylation of cathepsin B. The role of the primary structure of the latent precursor and of the carbohydrate moiety for cell-type-specific molecular forms of the enzyme. *Biochem. J.* **282**:577–582.
46. Maehr, R., et al. 2005. Asparagine endopeptidase is not essential for class II MHC antigen presentation but is required for processing of cathepsin L in mice. *J. Immunol.* **174**:7066–7074.
47. Katunuma, N., et al. 1999. Structure based development of novel specific inhibitors for cathepsin L and cathepsin S in vitro and in vivo. *FEBS Lett.* **458**:6–10.
48. Singh, V.P., et al. 2001. Phosphatidylinositol 3-kinase-dependent activation of trypsinogen modulates the severity of acute pancreatitis. *J. Clin. Invest.* **108**:1387–1395.
49. Gukovsky, I., et al. 2004. Phosphatidylinositide 3-kinase gamma regulates key pathologic responses to cholecystokinin in pancreatic acinar cells. *Gastroenterology.* **126**:554–566.
50. Saluja, A.K., et al. 1999. Secretagogue-induced digestive enzyme activation and cell injury in rat pancreatic acini. *Am. J. Physiol.* **276**:G835–G842.
51. Sherwood, M.W., et al. 2007. Activation of trypsinogen in large endocytic vacuoles of pancreatic acinar cells. *Proc. Natl. Acad. Sci. U. S. A.* **104**:5674–5679.
52. Blommaart, E.F., Krause, U., Schellens, J.P., Vreeling-Sindelarova, H., and Meijer, A.J. 1997. The phosphatidylinositol 3-kinase inhibitors wortmannin and LY294002 inhibit autophagy in isolated rat hepatocytes. *Eur. J. Biochem.* **243**:240–246.
53. Waterford, S.D., Kolodecik, T.R., Thrower, E.C., and Gorelick, F.S. 2005. Vacuolar ATPase regulates zymogen activation in pancreatic acini. *J. Biol. Chem.* **280**:5430–5434.
54. Kawai, A., Uchiyama, H., Takano, S., Nakamura, N., and Ohkuma, S. 2007. Autophagosome-lysosome fusion depends on the pH in acidic compartments in CHO cells. *Autophagy.* **3**:154–157.
55. Boland, B., et al. 2008. Autophagy induction and autophagosome clearance in neurons: relationship to autophagic pathology in Alzheimer's disease. *J. Neurosci.* **28**:6926–6937.
56. Kovacs, J., Laszlo, L., and Kovacs, A.L. 1988. Regression of autophagic vacuoles in pancreatic acinar, seminal vesicle epithelial, and liver parenchymal cells: a comparative morphometric study of the effect of vinblastine and leupeptin followed by cycloheximide treatment. *Exp. Cell Res.* **174**:244–251.
57. Luthen, R., Niederau, C., Niederau, M., Ferrell, L.D., and Grendell, J.H. 1995. Influence of ductal pressure and infusates on activity and subcellular distribution of lysosomal enzymes in the rat pancreas. *Gastroenterology.* **109**:573–581.
58. Lu, S.C., et al. 2003. Role of S-adenosylmethionine in two experimental models of pancreatitis. *FASEB J.* **17**:56–58.
59. Uchiyama, Y., and Saito, K. 1982. A morphometric study of 24-hour variations in subcellular structures of the rat pancreatic acinar cell. *Cell Tissue Res.* **226**:609–620.
60. Sreebny, L.M., and Johnson, D.A. 1969. Diurnal variation in secretory components of the rat parotid gland. *Arch. Oral Biol.* **14**:397–405.
61. Gukovskaya, A.S., Gukovsky, I., Jung, Y., Mouria, M., and Pandol, S.J. 2002. Cholecystokinin induces caspase activation and mitochondrial dysfunction in pancreatic acinar cells. Roles in cell injury processes of pancreatitis. *J. Biol. Chem.* **277**:22595–22604.
62. Webster, P. 2007. Microwave-assisted processing and embedding for transmission electron microscopy. In *Methods in molecular biology: electron microscopy. Methods and protocols.* J. Kuo, editor. Humana Press. Totowa, New Jersey, USA. 47–65.
63. Raraty, M., et al. 2000. Calcium-dependent enzyme activation and vacuole formation in the apical granular region of pancreatic acinar cells. *Proc. Natl. Acad. Sci. U. S. A.* **97**:13126–13131.
64. Otani, T., Chepilko, S.M., Grendell, J.H., and Gorelick, F.S. 1998. Codistribution of TAP and the granule membrane protein GRAMP-92 in rat caerulein-induced pancreatitis. *Am. J. Physiol.* **275**:G999–G1009.
65. Mortimore, G.E., Lardeux, B.R., and Adams, C.E. 1988. Regulation of microautophagy and basal protein turnover in rat liver. Effects of short-term starvation. *J. Biol. Chem.* **263**:2506–2512.
66. Ahlberg, J., Berkenstam, A., Henell, F., and Glaumann, H. 1985. Degradation of short and long lived proteins in isolated rat liver lysosomes. Effects of pH, temperature, and proteolytic inhibitors. *J. Biol. Chem.* **260**:5847–5854.
67. Claus, V., et al. 1998. Lysosomal enzyme trafficking between phagosomes, endosomes, and lysosomes in J774 macrophages. Enrichment of cathepsin H in early endosomes. *J. Biol. Chem.* **273**:9842–9851.
68. Gukovskaya, A.S., et al. 2002. Neutrophils and NADPH oxidase mediate intrapancreatic trypsin activation in murine experimental acute pancreatitis. *Gastroenterology.* **122**:974–984.
69. Kruger, B., Albrecht, E., and Lerch, M.M. 2000. The role of intracellular calcium signaling in premature protease activation and the onset of pancreatitis. *Am. J. Pathol.* **157**:43–50.